

# Structure and dynamics of the Benguela low-level coastal jet

Christina M. Patricola<sup>1,4</sup> · Ping Chang<sup>1,2,3</sup>

Received: 13 May 2016 / Accepted: 29 November 2016 / Published online: 22 December 2016  
© Springer-Verlag Berlin Heidelberg 2016

**Abstract** Generations of coupled atmosphere–ocean general circulation models have been plagued by persistent warm sea surface temperature (SST) biases in the southeastern tropical Atlantic. The SST biases are most severe in the eastern boundary coastal upwelling region and are sensitive to surface wind stress and wind stress curl associated with the Benguela low-level coastal jet (BLLCJ), a southerly jet parallel to the Angola–Namibia coast. However, little has been documented about this atmospheric source of oceanic bias. Here we investigate the characteristics and dynamics of the BLLCJ using observations, reanalyses, and atmospheric model simulations. Satellite wind products and high-resolution reanalyses and models represent the BLLCJ with two near-shore maxima, one near the Angola–Benguela front (ABF) at 17.5°S, and the other near 25–27.5°S, whereas coarse resolution reanalyses and models represent the BLLCJ poorly with a single, broad, more offshore maximum. Model experiments indicate that convex coastal geometry near the ABF supports the preferred location of the BLLCJ northern maximum by supporting conditions for a hydraulic expansion fan. Intraseasonal variability of the BLLCJ is associated with large-scale

variability in intensity and location of the South Atlantic subtropical high through modulation of the low-level zonal pressure gradient.

**Keywords** Low-level coastal jet · Benguela coastal upwelling system · SST bias · Hydraulic expansion fan

## 1 Introduction

The Benguela upwelling system, which sustains cold, nutrient-rich water along the coast of southwestern Africa and supports abundant fisheries, plays a major role in determining the spatial pattern of regional sea surface temperature (SST). The ocean circulation is characterized by the cool northward Benguela Current and warm southward Angola Current, which converge near 15°S–17°S to form a strong SST gradient named the Angola–Benguela front (ABF) (Rouault et al. 2007 and references therein). The Benguela current and upwelling are driven by strong southerly surface winds associated with an atmospheric low-level coastal jet (LLCJ), the Benguela LLCJ (BLLCJ). Although the BLLCJ plays an important role in supporting the Benguela upwelling system, relatively little has been documented about its characteristics and variability. An introduction of the BLLCJ described a single broad wind maximum located at 1000–925 hPa, 17°S–32°S, and ~6° longitude offshore based on coarse resolution reanalysis (Nicholson 2010). However as shown in this study, coarse resolution reanalysis is insufficient to accurately depict the jet structure, which is characterized by two distinct maxima according to high-resolution satellite wind products and finer resolution reanalyses.

There is strong motivation to understand the BLLCJ characteristics since representation of the jet in

✉ Christina M. Patricola  
patricola@tamu.edu

<sup>1</sup> Department of Atmospheric Sciences, Texas A&M University, College Station, TX, USA

<sup>2</sup> Department of Oceanography, Texas A&M University, College Station, TX, USA

<sup>3</sup> Physical Oceanography Laboratory/Qingdao Collaborative Innovation Center of Marine Science and Technology, Ocean University of China, Qingdao, China

<sup>4</sup> Climate and Ecosystem Sciences Division, Lawrence Berkeley National Laboratory, Berkeley, CA, USA

atmospheric models is one known source of the persistent warm SST bias in the southeastern tropical Atlantic (SETA) in coupled atmosphere–ocean general circulation model (AOGCM) and ocean model simulations (Grodsky et al. 2012; Small et al. 2015; Milinski et al. 2016; Kurian et al. 2016, in preparation). The SST bias is most severe near the ABF, reaching 6°C in the multi-model average of AOGCMs from the Coupled Model Intercomparison Project Phase 5 (CMIP5) of the Intergovernmental Panel on Climate Change (IPCC), and extends over the SETA and eastern equatorial Atlantic (Xu et al. 2014a, b). The biases in these regions may each arise from separate processes (Grodsky et al. 2012; Xu et al. 2014a, b; Toniazzo and Woolnough 2014; Richter 2015; Zuidema et al. 2016). The eastern equatorial bias has been linked to a springtime westerly equatorial trade wind bias, a dry Amazon bias, and a wet Congo Basin precipitation bias (DeWitt 2005; Chang et al. 2007; Richter and Xie 2008; Wahl et al. 2011; Richter et al. 2012; Patricola et al. 2012). In the SETA, the warm SST bias in the open ocean has been attributed to errors in representation of incident solar radiation associated with simulated marine stratus clouds, whereas the coastal SST bias has been attributed to problems with the ocean model, including insufficient upwelling, errors in mixing, overshooting of the Angola Current, a too-diffuse coastal thermocline, and insufficient model resolution (Hazeleger and Harsma 2005; Large and Danabasoglu 2006; Huang et al. 2007; Wahl et al. 2011; Xu et al. 2014a, b; Small et al. 2015). The coastal SST biases can also originate from different processes in different models, as suggested by decadal hindcasts with three AOGCMs that produced SST biases linked to errors in surface zonal wind, errors in incident short-wave fluxes, and strong regional wind–SST–precipitation coupling (Toniazzo and Woolnough 2014). Several studies have also demonstrated that the atmosphere, through the BLLCJ, is a large potential source of coastal SST bias in the SETA. Ocean model simulations show that the ABF location is strongly controlled by changes in the meridional location of wind stress curl (Colberg and Reason 2006), which controls the southward flow offshore of the eastern-boundary current system (Small et al. 2015). In addition, the oceanic current system is sensitive to the location of the wind stress curl in relation to the coast (Fennel et al. 2012). Similarly, the local wind stress curl and the detailed coastal wind structure play an important role in determining the ABF location and Benguela upwelling and in reducing coastal SST bias (Small et al. 2015). Furthermore, Milinski et al. (2016) found that misrepresentation of the surface wind at low atmospheric horizontal resolution is a major source of coastal SST bias in the southeastern tropical Atlantic, and

that high atmospheric horizontal resolution substantially reduces the SST bias.

An understanding of well-observed LLCJs, such as those along the California and South American coasts, provides a foundation for understanding the relatively understudied BLLCJ. LLCJs are atmospheric jets that flow Equatorward and parallel to and along coastlines, and tend to occur in eastern boundary upwelling regions. Observations indicate that the California LLCJ is driven by thermal wind processes associated with the thermal contrast between land and ocean (Zemba and Friehe 1987; Gerber et al. 1989; Parish 2000), which tends to be strong in eastern boundary coastal upwelling regions due to the upwelling of cold deep ocean water. These conditions support the cool, stable, and well-mixed marine atmospheric boundary layer (MABL) necessary for LLCJ formation. During LLCJ events, the MABL is capped by a sloping temperature inversion that decreases in height toward the coast (e.g., Zemba and Friehe 1987; Beardsley et al. 1987; Parish 2000) and is often associated with subsidence from the eastern portion of the North Pacific High in the California LLCJ case (Neiburger et al. 1961; Parish 2000; Rahn and Parish 2007).

Like the California LLCJ, the South American LLCJ is supported by a near-surface pressure gradient perpendicular to the coast, where a cool stable MABL forms adjacent to warm land (Garreaud and Muñoz 2005; Muñoz and Garreaud 2005). The very steep coastal terrain is important in the determining the dynamics of the South American LLCJ, because it prevents an easterly low-level wind that would geostrophically balance the cross-shore pressure gradient, resulting in an acceleration of the meridional LLCJ flow (Muñoz and Garreaud 2005).

Although LLCJs are driven primarily by land–ocean thermal contrast and do not require topographic features to form (Parish 2000), topographic influences can play an important role in determining smaller-scale jet maxima in observations and according to hydraulic theory (Winant et al. 1988; Samelson 1992; Rogers et al. 1998; Dorman and Koračin 2008). The previously discussed conditions favorable for LLCJs, i.e., a cool, stable coastal MABL capped by a sloping temperature inversion adjacent to warm coastal terrain, can establish the conditions for hydraulic dynamics, as the LLCJ flow is bounded by coastal topography, the inversion at the top of the MABL, and the ocean surface. When the flow is sufficiently fast, characterized as supercritical by a Froude number greater than 1, convex variations in coastline geometry induce a hydraulic expansion fan downwind, and a hydraulic compression jump upwind of the cape or point (Dorman 1985; Winant et al. 1988; Samelson 1992). A hydraulic expansion fan is characterized by a lateral spreading of flow and thinning of the MABL, which leads to enhanced wind speed and reduced marine stratus cloud cover

through adiabatic warming associated with descending motion; likewise, a hydraulic jump induced by flow upwind of convex coastal geometry that is blocked by the terrain, is characterized by a deepening of the MABL, reduced wind speed, and increased marine stratus cloud cover (Winant et al. 1988; Samelson 1992). Frictional effects are important in determining the spatial pattern of the wind maxima in the hydraulic model (Samelson 1992).

With motivation to ultimately reduce coupled model SST biases in the Benguela coastal upwelling region, one of the high-priority recommendations of the U.S. CLIVAR Working Group on Eastern Tropical Ocean Synthesis (Zuidema et al. 2016), the purpose of this study is to (1) describe the structure and variability of the BLLCJ, (2) document biases in the BLLCJ in models and reanalyses, and (3) understand the dynamics of the BLLCJ, including the cause of its double maximum structure. We note that although the South American and Benguela LLCJs occur under similar MABL and coastal terrain conditions, albeit with higher terrain in the South American case, the two LLCJs are characterized by different jet structures, with a single broad maximum in the South American case and two maxima in the Benguela case (Fig. 1), raising the question, *what determines the double maximum structure of the Benguela LLCJ?* We hypothesize on the basis of hydraulic theory that the BLLCJ structure is closely related to coastal geometry, which is relatively smooth in the case of the South American LLCJ and more complicated in the BLLCJ case. In a follow-up paper we will demonstrate that the coastal SST bias in the SETA is highly dependent on the representation of the BLLCJ using regional ocean model

simulations forced with atmospheric reanalysis and the regional atmosphere model output described in Sect. 2 (Kurian et al. 2016, in preparation).

## 2 Datasets

### 2.1 Observational and reanalysis products

This section first describes the observational products used in this study, which are summarized in Table 1. The fine-resolution satellite-based Scatterometer Climatology of Ocean Winds (SCOW) (Risien and Chelton 2008) is considered to be the gridded product that is closest to the truth, although uncertainty is present in near-coast scatterometer data caused by land contamination. Data from the microwave radiometers used to derive satellite-based ocean surface wind are typically unavailable within 100 km of the coastline (Yang et al. 2014). The SCOW is based on a harmonic analysis of the National Aeronautical and Space Administration (NASA) Quick Scatterometer (QuikSCAT) ocean surface winds and provides a gridded monthly climatology (September 1999–October 2009) of 10-m wind and wind stress vectors, curl, and divergence at  $0.25^\circ \times 0.25^\circ$  resolution with near-global coverage.

A second ocean wind product, the Cross-Calibrated Multi-Platform (CCMP) Ocean Surface Wind Vector Analyses (Atlas et al. 2011), combines multiple sources of microwave satellite data, in-situ measurements, and the European Centre for Medium-Range Weather Forecasts (ECMWF) ERA-40 Reanalysis and ECMWF Operational analysis using a Variational Analysis Method. The CCMP product includes gridded, 6-hourly,  $0.25^\circ \times 0.25^\circ$

**Fig. 1** Meridional wind at 10-m ( $\text{m s}^{-1}$ ; blue) from the Scatterometer Climatology of Ocean Winds (SCOW) climatology and terrain height (km; orange) from the NCEP CFSR over the **a** Benguela and **b** South American coastal upwelling regions

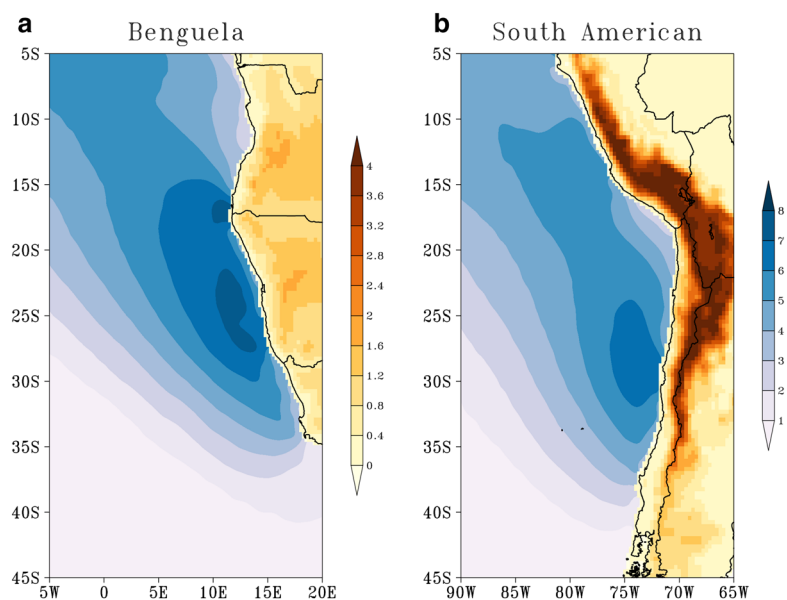


**Table 1** Summary of observational and reanalysis products

Data product	Variables	Surface field resolution	Time period
SCOW Scatterometer Climatology of Ocean Winds	10-m ocean wind and wind stress vectors and derivatives	$0.25^\circ \times 0.25^\circ$	Sep 1999–Oct 2009
CCMP Cross-Calibrated Multi-Platform Ocean Surface Wind Vector Analyses	10-m wind	$0.25^\circ \times 0.25^\circ$	Jul 1987–Dec 2011
CORE-II Coordinated Ocean-ice Reference Experiments version 2	Air-sea momentum, heat, and fresh-water fluxes	$\sim 1.875^\circ \times \sim 1.875^\circ$	1948–2009
NCEP CFSR Climate Forecast System Reanalysis	3-D atmospheric and ocean reanalysis	$\sim 0.3125^\circ \times \sim 0.3125^\circ$	1979–2010
JRA-55 Reanalysis Japanese 55-year Reanalysis	3-D atmospheric reanalysis	$\sim 55$ km	1958–present
MERRA Modern Era Retrospective-analysis for Research and Applications	3-D atmospheric reanalysis	$2/3^\circ$ longitude $\times$ $1/2^\circ$ latitude	1979–present
ECMWF-Interim Reanalysis	3-D atmospheric reanalysis	$\sim 80$ km	1979–present
NCEP/NCAR Reanalysis	3-D atmospheric reanalysis	$\sim 1.875^\circ \times \sim 1.875^\circ$	1949–present
NCEP-II Reanalysis	3-D atmospheric reanalysis	$\sim 1.875^\circ \times \sim 1.875^\circ$	1979–present

resolution 10-m wind vectors over the ocean surface from July 1987 through December 2011. This study uses the fully-assimilated gap-free monthly averaged surface wind fields (L3.5).

A set of global, gridded air-sea momentum, heat, and fresh-water fluxes commonly used as atmospheric forcing for ocean models is provided by the Coordinated Ocean-ice Reference Experiments version 2 (CORE-II; Large and Yeager 2008), which was coordinated by the Climate and Ocean: Variability, Predictability and Change (CLIVAR) Working Group on Ocean Model Development. The CORE-II covers 1948 through 2009 and includes 6-hourly fields on a  $\sim 1.875^\circ \times \sim 1.875^\circ$  grid. Near surface winds are based on QuikSCAT and the National Centers for Environmental Prediction/ National Center for Atmospheric Research (NCEP/NCAR) Reanalysis, which is described below.

We next present the global, gridded atmospheric reanalysis data sets, in order from fine to coarse resolution, that are used in this study (Table 1). The most recent

reanalysis of NCEP, and one of the finest resolution global reanalyses to date, is the Climate Forecast System Reanalysis (CFSR; Saha et al. 2010), with a horizontal resolution of  $\sim 38$  km and 64 levels in the vertical. The CFSR includes coupling with the Geophysical Fluid Dynamics Laboratory (GFDL) Modular Ocean Model (MOM) and a sea ice model, and includes both atmospheric and oceanic reanalysis data from 1979 to 2010. NASA QuikSCAT and Naval Research Laboratory WindSat ocean surface winds are assimilated in the CFSR. This study uses monthly averaged data on a  $0.5^\circ \times 0.5^\circ$  upper-air grid and  $\sim 0.3125^\circ \times \sim 0.3125^\circ$  surface grid.

The Japanese 55-year Reanalysis (JRA-55; Kobayashi et al. 2015) of the Japan Meteorological Agency provides atmospheric reanalysis at a fine resolution of  $\sim 55$  km. Like the CFSR, the JRA-55 assimilates scatterometer ocean surface winds including QuikSCAT. The JRA-55 includes improvements from the previous reanalysis, JRA-25, and covers 1958 through present.

**Table 2** Summary of regional climate model simulations

Simulation name	Horizontal resolution (km)	Time step (s)	Domain	Coastline	Time period	Cumulus
3 km	3	12	Region	Actual	1 Mar–1 Nov 2011	None
9 km	9	30	Region	Actual	1 Jan 2005–1 Jan 2006	ZM
9 km	9	30	Region	Actual	1 Jan 2005–1 Jan 2010	None
27 km	27	45	Region	Actual	1 Jan 2005–1 Jan 2015	ZM
Modified coast	27	45	Region	Modified	1 Jan 2005–1 Jan 2015	ZM
81 km	81	60	Region	Actual	1 Jan 2005–1 Jan 2010	ZM
243 km	243	300	Basin	Actual	1 Jan 2005–1 Jan 2010	ZM

ZM denotes Zhang McFarlane cumulus scheme

The Modern Era Retrospective-analysis for Research and Applications (MERRA; Rienecker et al. 2011) of NASA is an atmospheric reanalysis that covers the satellite era, 1979 through present, with surface data on a  $2/3^\circ$  longitude  $\times$   $1/2^\circ$  latitude grid. The MERRA assimilates surface wind data from QuikSCAT and the European Remote Sensing Satellite (ERS) generations 1 and 2.

The ECMWF-Interim Reanalysis (Dee et al. 2011) is an atmospheric reanalysis product at  $\sim 80$  km resolution that covers 1979 through present. Like MERRA, ECMWF-Interim assimilates QuikSCAT, ERS-1, and ERS-2 data for ocean surface wind.

One of the earliest atmospheric reanalysis products is the NCEP/NCAR Reanalysis (Kalnay et al. 1996), which provides 6-hourly and monthly averaged upper-atmospheric data on a  $2.5^\circ \times 2.5^\circ$  grid and surface fields on an approximately  $1.875^\circ \times 1.875^\circ$  grid for 1949 through present. The NCEP/NCAR Reanalysis is produced by assimilating quality-controlled land surface, ship, rawinsonde, pibal, aircraft, and satellite data within a Climate Data Assimilation System that uses the T62/28-level NCEP global spectral

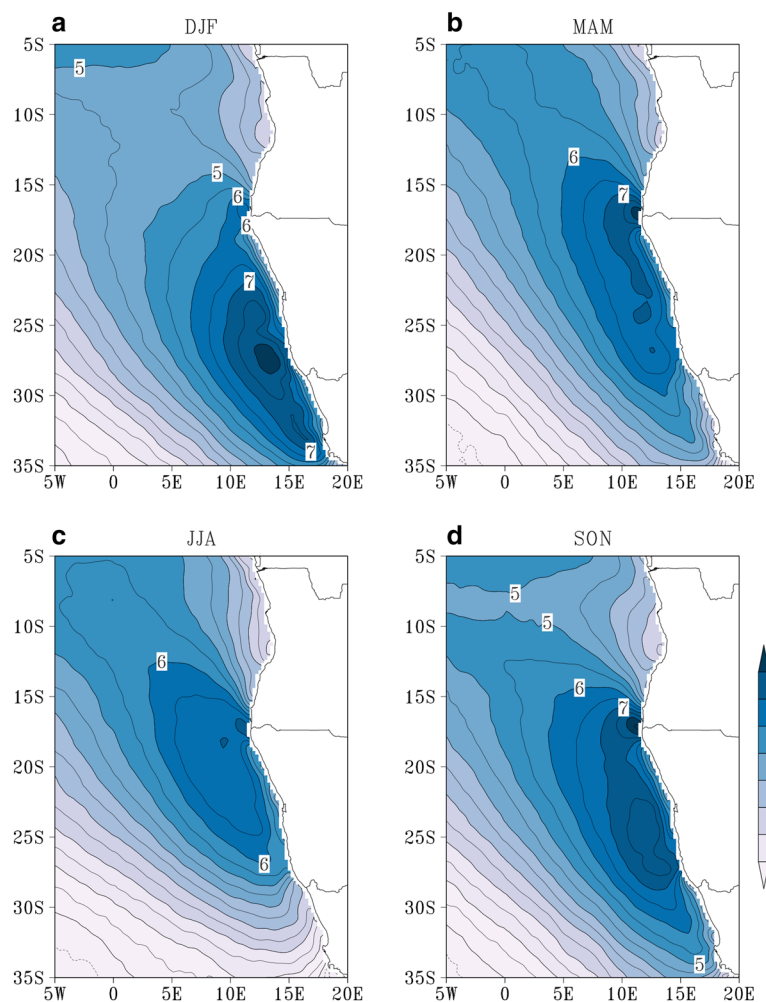
model. Near surface winds are classified as category B, meaning that the variable is strongly based on observational data, but is also strongly influenced by the model.

The NCEP/NCAR reanalysis was followed by the NCEP-Department of Energy (DOE) Atmospheric Model Intercomparison Project (AMIP)-II Reanalysis (NCEP-II; Kanamitsu et al. 2002), which includes upgrades to the forecast model and error fixes. The NCEP-II Reanalysis covers 1979 through present, and 6-hourly and monthly-averaged data are available on the same horizontal grids as the NCEP Reanalysis.

## 2.2 Regional and global climate model simulations

Numerical experiments are conducted with the Weather Research and Forecasting (WRF; Skamarock et al. 2008) model version 3.5.1, which is developed and maintained by NCAR. WRF is a nonhydrostatic terrain-following regional climate model. A suite of simulations is performed with several horizontal resolutions, including 3, 9, 27, 81, and 243 km, and a resolution-dependent model time step

**Fig. 2** Meridional wind at 10-m ( $\text{m s}^{-1}$ ) from the SCOW climatology averaged **a** Dec-Jan-Feb, **b** Mar-Apr-May, **c** Jun-Jul-Aug, and **d** Sep-Oct-Nov. White indicates no data



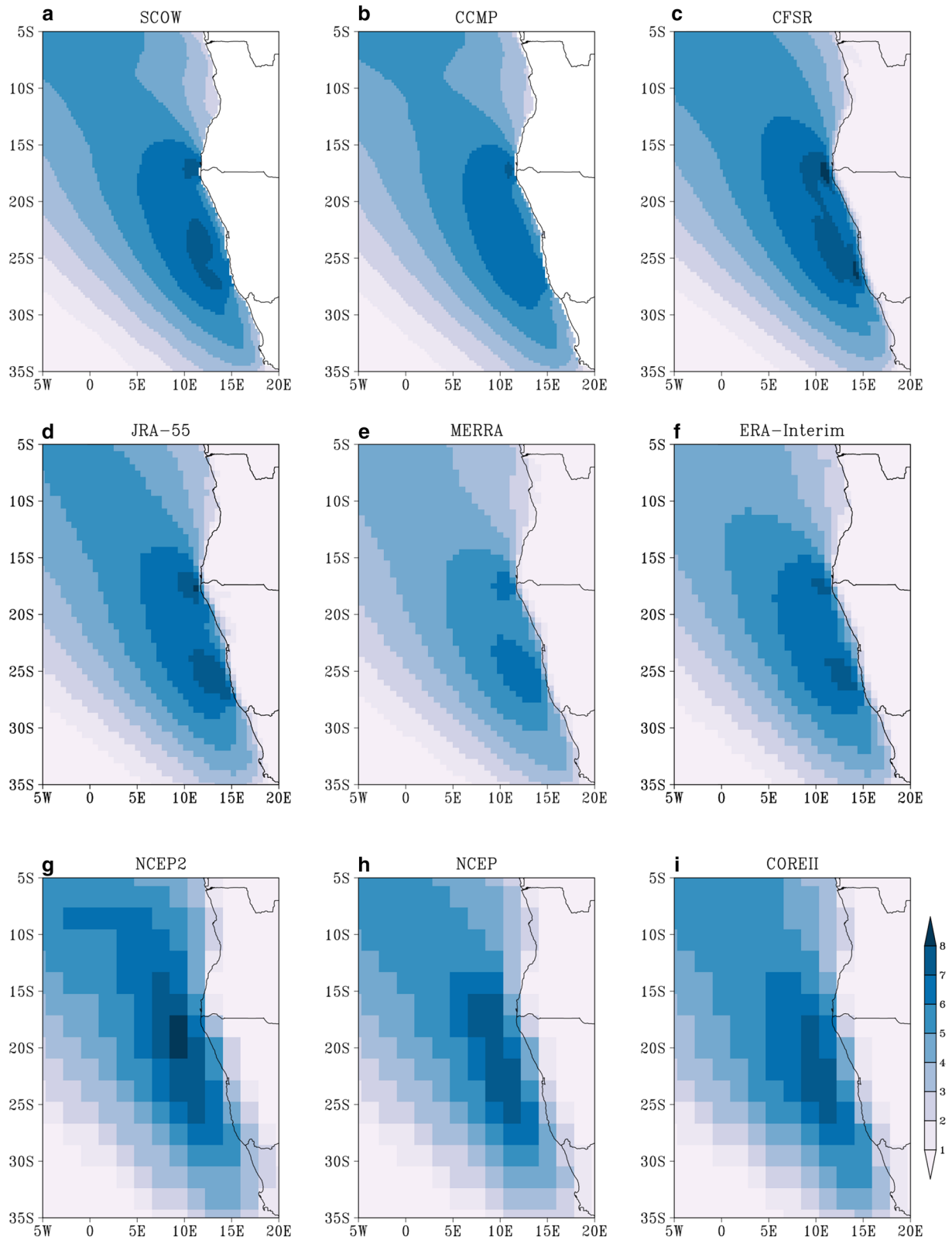


**Fig. 3** Meridional wind at 10-m ( $\text{m s}^{-1}$ ) averaged from the **a** SCOW climatology (September 1999–October 2009) and from the 1999–2009 average of the **b** CCMP data set, **c** NCEP CFSR, **d** JRA-

**55**, **e** MERRA, **f** ERA-Interim Reanalysis, **g** NCEP-II Reanalysis, **h** NCEP Reanalysis, and **i** CORE-II data set. *White* indicates no data

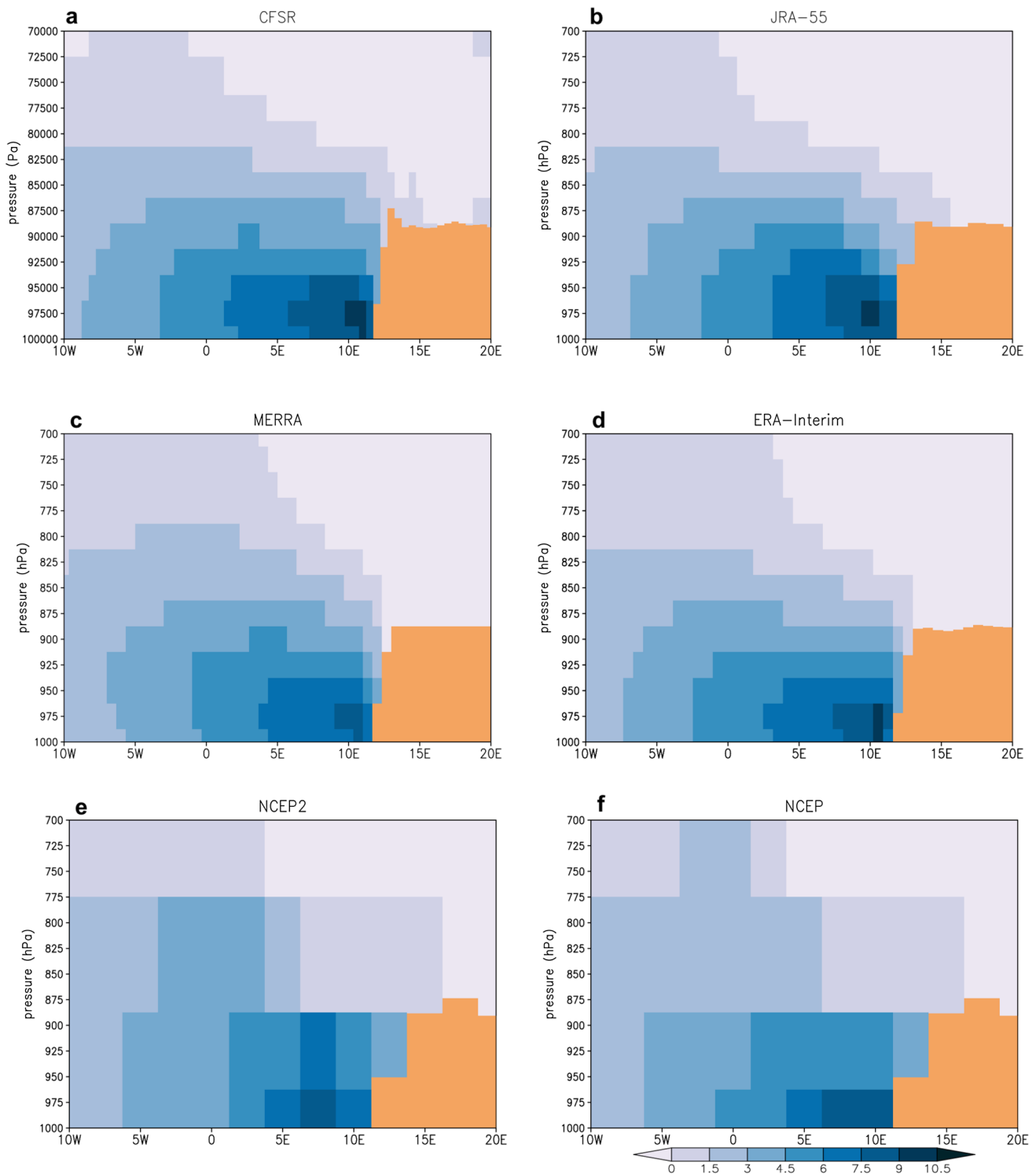
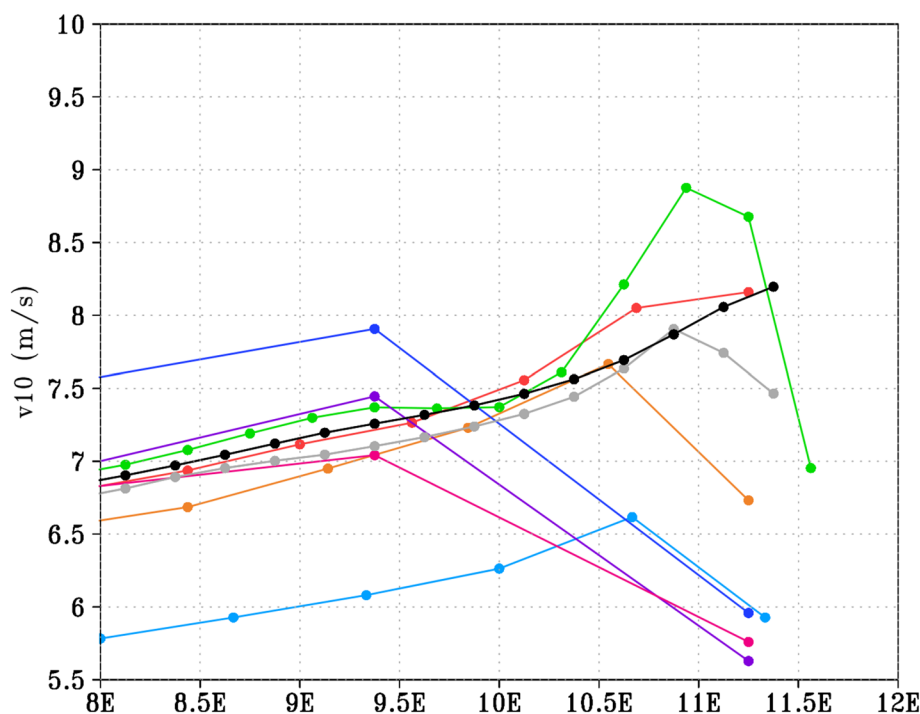


**Fig. 4** Vertical cross sections of meridional wind ( $\text{m s}^{-1}$ ) at the grid point closest to  $17.5^\circ\text{S}$  averaged Mar–Apr–May 1988–2009 from the **a** NCEP CFS, **b** JRA-55, **c** MERRA, **d** ERA-Interim, **e** NCEP-II and **f** NCEP Reanalyses. Land is shaded brown

(Table 2); all simulations are configured with 32 levels in the vertical determined by WRF’s default configuration. Simulations use the following physical parameterizations: Community Atmosphere Model (CAM) Microphysics,

Rapid Radiative Transfer Model for General Circulation Models (RRTMG) radiation, Yonsei University (YSU) planetary boundary layer, Monin–Obukhov surface scheme, and the Noah land-surface model. Simulations

**Fig. 5** Meridional wind at 10-m ( $\text{m s}^{-1}$ ) at the grid point closest to  $17.5^\circ\text{S}$  from the Mar–Apr–May 2000–2009 climatology from the SCOW data set (black), CCMP data set (grey), JRA-55 (red), MERRA (orange), NCEP CFSR (green), ECMWF-Interim Reanalysis (light blue), NCEP-II Reanalysis (dark blue), NCEP Reanalysis (purple), and CORE-II (magenta). Data are shown over ocean only



configured at 27 km resolution and coarser use the Zhang McFarlane cumulus scheme, and no cumulus parameterization is used in the 3 km resolution simulation. Simulations are run at 9 km resolution both with the Zhang McFarlane cumulus scheme and without. All simulations are run on a southeastern Atlantic “regional” domain covering  $52^\circ\text{S}$ – $32^\circ\text{N}$  and  $22^\circ\text{W}$ – $25^\circ\text{E}$ , except for the 243 km resolution simulation, which is run on an Atlantic sector “basin” domain covering  $52^\circ\text{S}$ – $32^\circ\text{N}$  and  $85^\circ\text{W}$ – $25^\circ\text{E}$ . Model output is saved every 3 h.

Initial and lateral boundary conditions are prescribed from 6-hourly  $2.5^\circ \times 2.5^\circ$  NCEP-II Reanalysis (Kanamitsu et al. 2002). SST is based on daily  $0.25^\circ \times 0.25^\circ$  NOAA-OI V2 SST (Reynolds et al. 2002) for simulations configured with a horizontal resolution of 27 km and coarser, and daily  $0.011^\circ$  resolution Group for High Resolution Sea Surface Temperature (GHRSSST) Level 4 Multiscale Ultrahigh Resolution (MUR) SST (Chin et al. 2013) for simulations at 3 and 9 km resolution. All simulations are initialized on 00z 1 January 2005 and integrated through 1 January 2010, except the 27 km resolution simulation, which extends though 1 January 2015, the 9 km resolution simulation that employs a cumulus parameterization, which is run through 1 January 2006, and the 3 km resolution simulation, which is initialized on 00z 1 March 2011 and integrated through 1 November 2011 due to high computational cost (Table 2).

An additional simulation is performed to investigate the cause of the double maximum structure of the Benguela jet. In this experiment, the African coastline is altered such

that the convex coastal geometry near  $17.5^\circ\text{S}$  is removed and terrain height is set to zero over regions where land is changed to ocean, as explained in Sect. 5b. In addition, surface properties including albedo and surface roughness are modified accordingly where land is changed to ocean. This simulation is performed at 27 km horizontal resolution.

In addition to the regional climate model simulations, 42 global climate model simulations from the Coupled Model Intercomparison Project Phase 5 (CMIP5) of the Intergovernmental Panel on Climate Change (IPCC) are presented (Taylor et al. 2012). We consider a multi-model ensemble the historical AMIP integrations with prescribed observed greenhouse gas concentrations and SST. Details about the models are summarized in Table 1 of Xu et al. (2014b).

### 3 Benguela LLCJ structure

An early study of the Benguela LLCJ describes a jet that is oriented parallel to the Namib coast, covers  $17^\circ\text{S}$ – $32^\circ\text{S}$ , and is strongest in October with maximum wind speeds approximately  $6^\circ$  longitude offshore and at 1000 hPa, according to the NCEP Reanalysis (Nicholson 2010). However, representation of the BLLCJ is highly dependent on reanalysis product, as shown in this section. Here we present characteristics of the BLLCJ from several reanalyses to improve our understanding of the jet and identify biases in reanalyses, relative to satellite-based observations, that



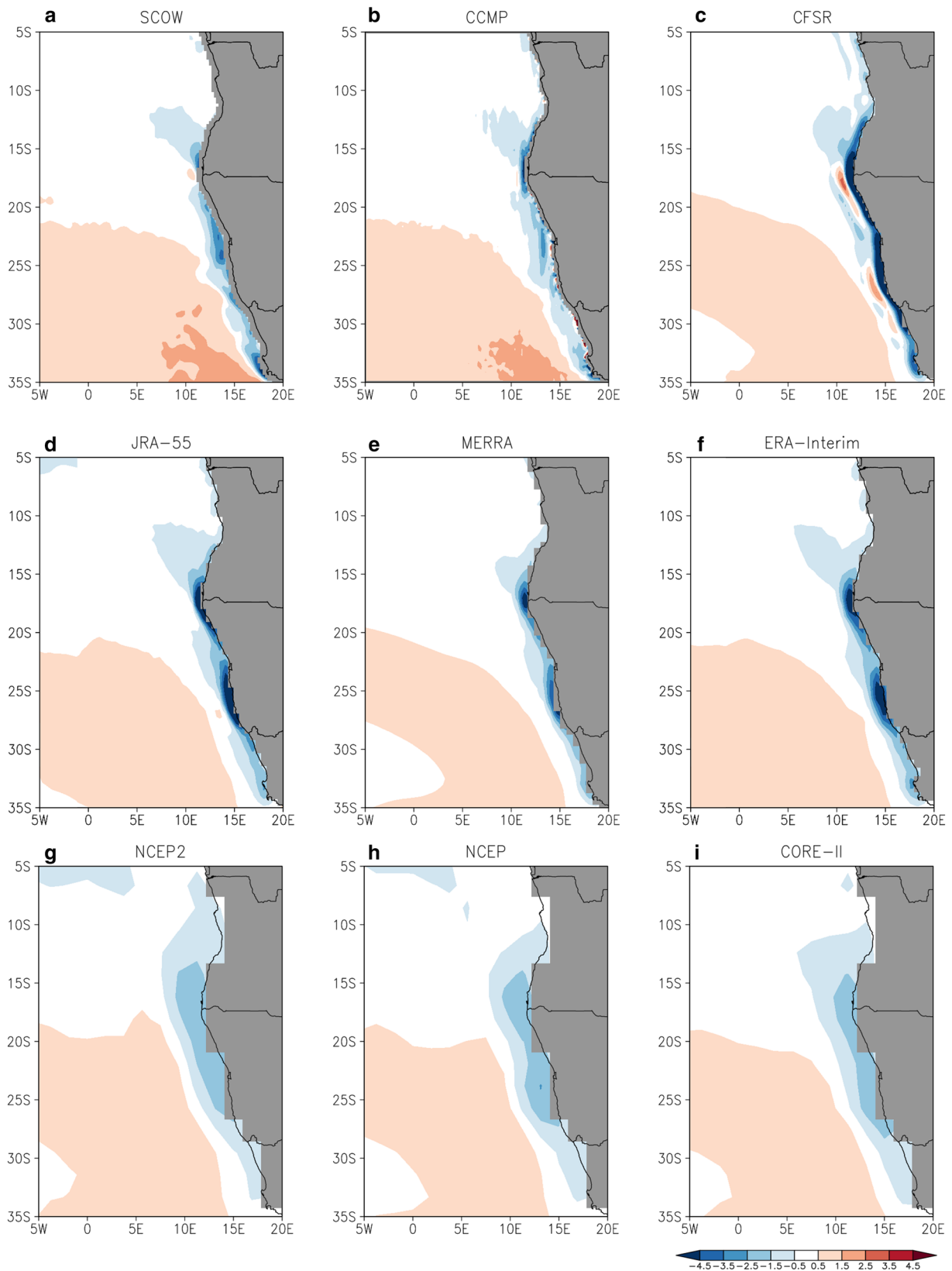


**Fig. 6** Wind stress curl at 10-m ( $10^{-7} \text{ N m}^{-3}$ ) from the **a** SCOW climatology (September 1999–October 2009) and from the 1999–2009 average of the **b** CCMP data set, **c** NCEP CFSR, **d** JRA-55, **e**

**MERRA**, **f** ERA-Interim Reanalysis, **g** NCEP-II Reanalysis, **h** NCEP Reanalysis, and **i** CORE-II data set. Grey indicates land or missing data

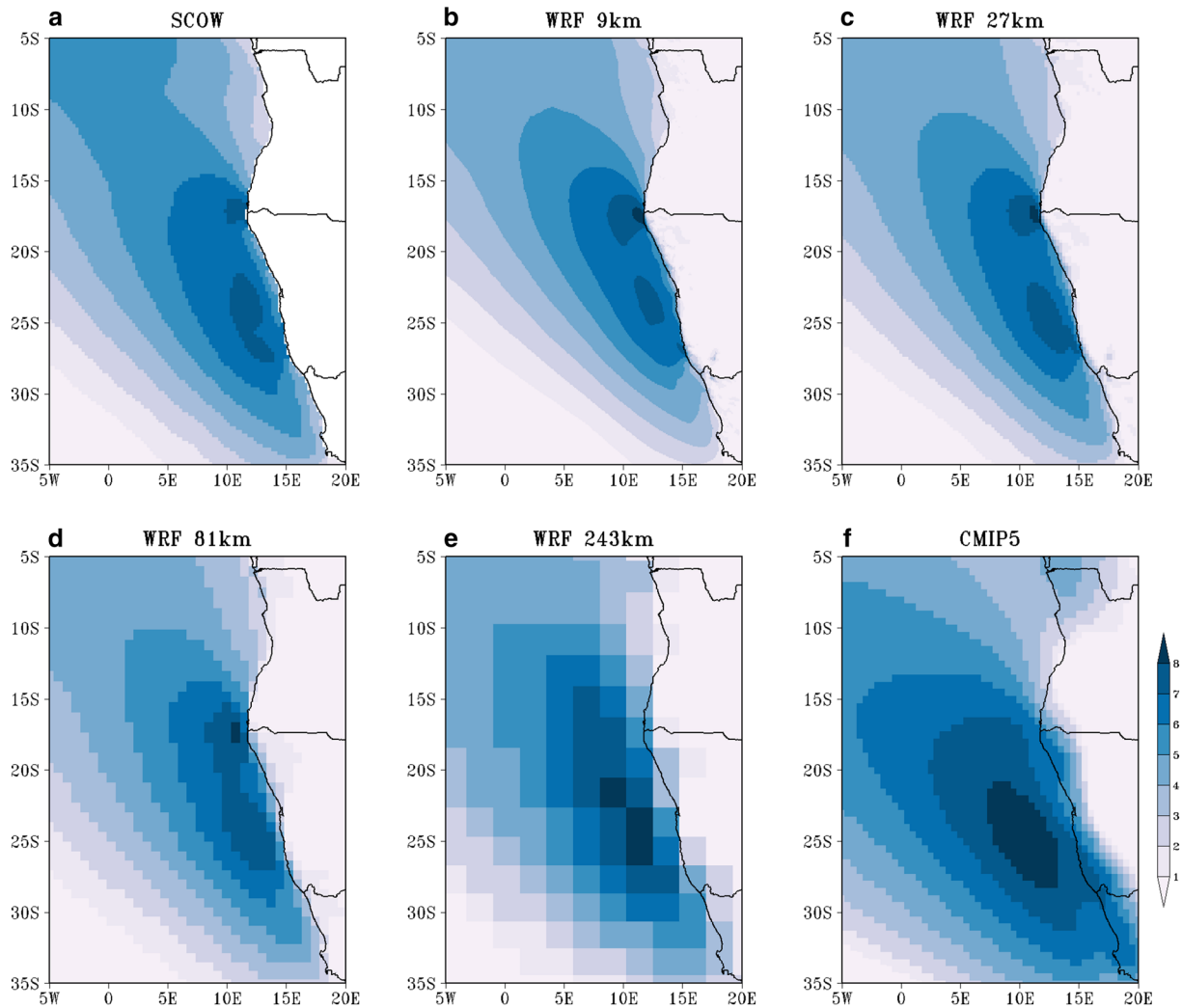


**Fig. 7** Meridional wind at 10-m ( $\text{m s}^{-1}$ ) from the **a** SCOW climatology (September 1999–October 2009), the January 2005–December 2009 average of WRF simulations at horizontal resolution of **b** 9 km,

**c** 27 km, **d** 81 km, and **e** 243 km, and the **f** January 1984–December 2004 average from the CMIP5 multi-model ensemble

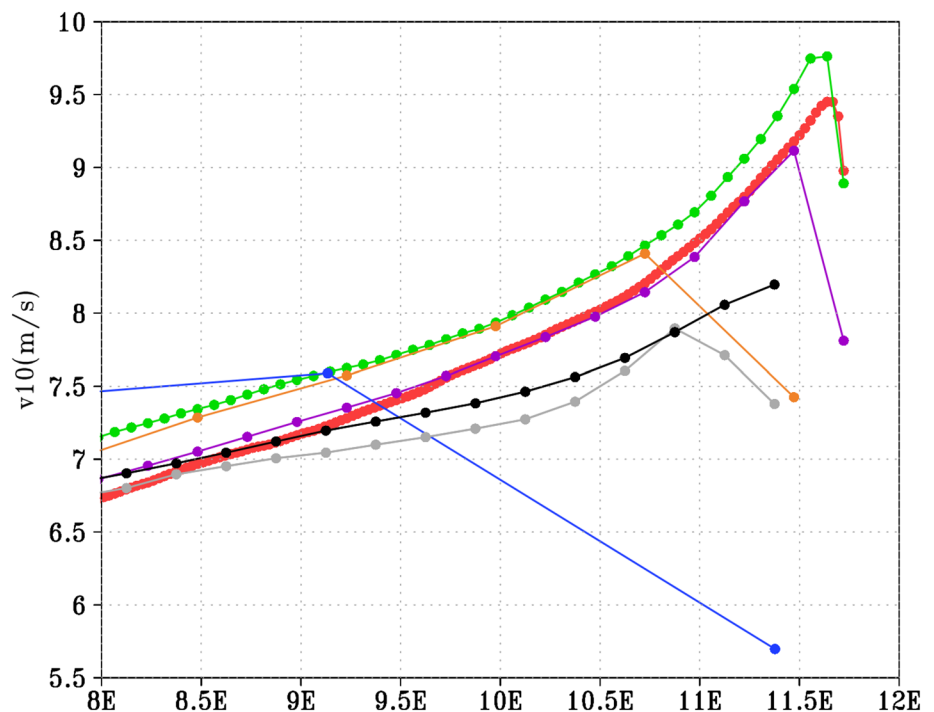
would be a source of error when used as atmospheric forcings for ocean model simulations.

Unlike the NCEP Reanalysis (Nicholson 2010), the SCOW satellite product shows a BLLCJ that has two seasonally-dependent maxima (Fig. 2), a quasi-permanent northern maximum at  $17.5^{\circ}\text{S}$  that coincides with the Cunene upwelling cell (Lutjeharms and Meeuwis 1987) and ABF, and a southern maximum at  $25^{\circ}\text{S}$ – $30^{\circ}\text{S}$  that coincides with the Lüderitz upwelling cell (Lutjeharms and Meeuwis 1987). The northern maximum is located near the coast and is strongest in austral autumn and spring (Fig. 2b, d), whereas the southern maximum is a few degrees of longitude offshore and is strongest in austral summer and spring (Fig. 2a, d). The BLLCJ is weakest in austral winter when there is no southern maximum is the seasonal mean

(Fig. 2c). These two distinct jet maxima are present in the annual average of the SCOW product (Fig. 3a).

The representation of the BLLCJ in the 1999–2009 annual average (the period of overlap among the data sets) is quite different among reanalyses and depends highly on horizontal resolution. In general, reanalyses with horizontal resolution finer than  $\sim 2^{\circ}$  (Fig. 3a–f) represent the two BLLCJ maxima seen in the SCOW product, with the northern maximum anchored at  $17.5^{\circ}\text{S}$  and some differences in wind speed magnitude and offshore distance of the southern jet maximum, whereas all products at about  $2^{\circ}$  resolution represent the BLLCJ as a single broad maximum (Fig. 3g–i). The CCMP analysis (Fig. 3b) is characterized by two 10-m meridional wind speed maxima in similar locations compared with the

**Fig. 8** Similar to Fig. 5, except from the Mar–Apr–May climatology from the SCOW data set (*black*) and CCMP data set (*grey*), and WRF simulations at horizontal resolution of 3 km (*red*), 9 km (*green*), 27 km (*purple*), 81 km (*orange*), and 243 km (*blue*). The SCOW covers 2000–2009, the WRF 3 km simulation covers 2011, and all other WRF simulations cover 2005–2009



SCOW (Fig. 3a), although the magnitudes are weaker. (The southern maximum is not visible in Fig. 3b due to the shading interval.) The CFSR (Fig. 3c) produces jet maxima that are stronger than those in SCOW, and also places the southern maximum nearer to the coast. The JRA-55 (Fig. 3d) represents the BLLCJ most closely to the SCOW (Fig. 3a), with similar magnitudes of wind speed but a slight difference in proximity of the southern maximum to the coast. Both MERRA and ERA-Interim (Fig. 3e, f) show a BLLCJ that is weaker than that in the SCOW (Fig. 3a) with again slight differences in proximity of the southern maximum to the coast, where there is uncertainty in scatterometer winds caused by land contamination. All three coarse resolution products, NCEP, NCEP-II, and CORE-II (Fig. 3g–i) represent the BLLCJ with one maximum between approximately 27.5°S and 20°S and lack the maximum that is located near 17.5°S in the finer resolution products. Although many of the reanalyses represent the BLLCJ with one broad wind maximum, the products that are closest to the truth, i.e., the satellite-based observations, indicate that the BLLCJ is indeed characterized by two distinct wind maxima.

For a complete view of the Benguela LLCJ structure, we consider vertical cross sections of the meridional wind over the northern jet region at 17.5°S from all products with upper-level data available. Discrepancies between the finer (Fig. 4a–d) vs. coarse resolution (Fig. 4e, f) reanalyses are clear, with fine resolution products placing the jet maximum at 975 hPa and near the steep topography, whereas

NCEP and NCEP-II show a more offshore jet maximum at 1000 hPa.

Simulated coastal SST and upwelling are sensitive to the near coast surface wind structure (Small et al. 2015), therefore we examine the profile of 10-m meridional wind within a few degrees of longitude from the African coast within the BLLCJ northern maximum (Fig. 5) during the peak SST bias in March–May (Richter and Xie 2008; Patricola et al. 2012). Whereas most reanalyses and observational products are in relative agreement offshore, the products produce vastly different wind profiles within about 2° of longitude from the coastline. Even those products based heavily on QuikSCAT ocean surface winds, the SCOW and CCMP, differ in placement of the wind maximum, with SCOW showing a maximum at the grid point adjacent to the coast and CCMP placing the maximum three grid points away from the coast (Fig. 5). Most higher resolution reanalyses, including NCEP CFSR, MERRA, and ERA-Interim, are qualitatively similar in pattern to the CCMP, but with different wind magnitudes, whereas the JRA-55 is more similar to the SCOW in placing the maximum wind speed adjacent to the coast. The coarse resolution products, NCEP-II, NCEP, and CORE-II, show wind profiles that are dramatically different from the other products, with maxima located several degrees of longitude (albeit two grid points) away from the coastline.

The location of the wind maximum relative to the coastline dictates wind stress curl, another quantity that strongly influences coastal SST and upwelling (Colberg

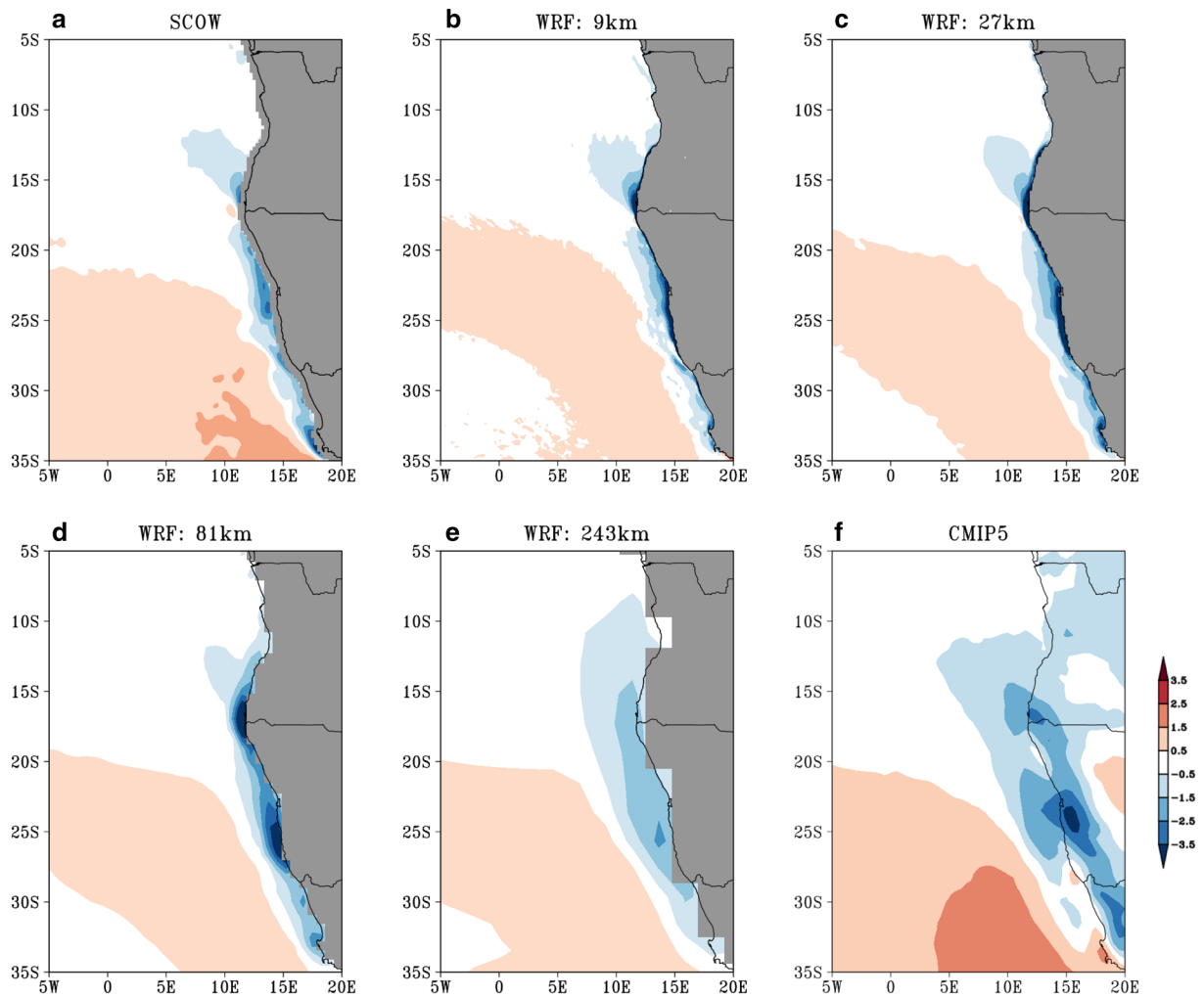


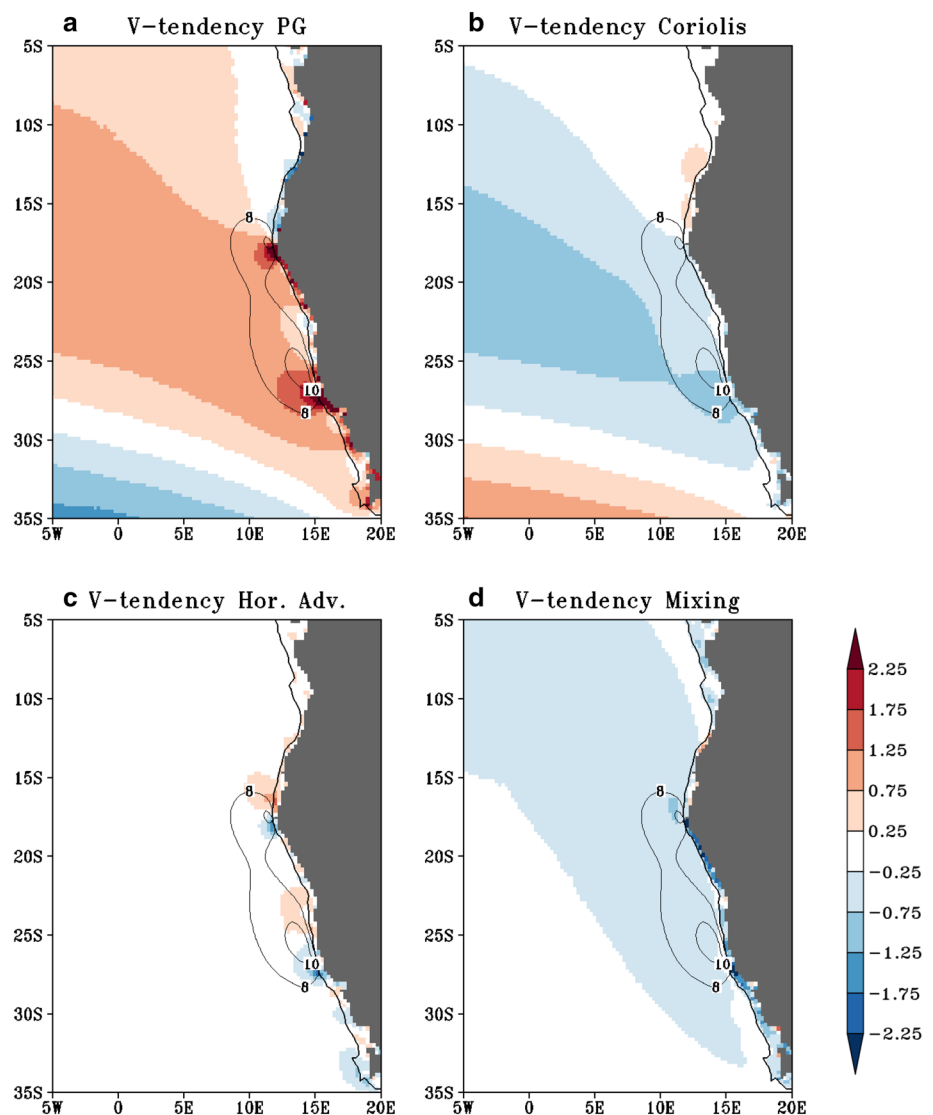
**Fig. 9** Wind stress curl at 10-m ( $10^{-7} \text{ N m}^{-3}$ ) from **a** the SCOW climatology, WRF simulations at horizontal resolution of **b** 9 km, **c** 27 km, **d** 81 km, and **e** 243 km, and the **f** CMIP5 multi-model ensemble.

WRF simulations are averaged January 2005–December 2009, and CMIP5 simulations are averaged January 1984–December 2004

and Reason 2006; Small et al. 2015). Seasonal variability in wind stress curl has also been linked to variability in meridional transport in the Benguela upwelling system (Junker et al. 2015). Representation of wind stress curl (Fig. 6), like Benguela LLCJ (Fig. 3), varies greatly among observational and reanalysis products and depends highly on product resolution. Even the two  $0.25^\circ$  satellite wind based products display notable differences, especially at the ABF near  $17.5^\circ\text{S}$  where SCOW places a local maximum (Fig. 6a) that is absent in the CCMP (Fig. 6b). In addition, there are differences in near-coast wind stress curl between SCOW and CCMP over the entire Benguela upwelling region, with CCMP showing sporadic positive values between  $22.5^\circ\text{S}$  and  $30^\circ\text{S}$  that are likely artifacts related to data availability issues

near the coast and uncertainty from land contamination of satellite data. Of the four relatively high-resolution reanalyses, three (Fig. 6d–f) most closely reproduce the qualitative wind stress curl field of the SCOW, with the notable exception of the weak maximum at  $17.5^\circ\text{S}$ , and all overestimate the magnitude of wind stress curl relative to the satellite products. The NCEP CFSR produces erroneous positive regions of wind stress curl offshore from the overestimated minima that hug the coastline (Fig. 6c), errors with the potential for substantial impacts on simulated SST. The wind stress curl in coarse resolution products, including the CORE-II data set that is commonly used as atmospheric forcing for ocean models, is poorly represented as a minimum that is weaker and spatially broader than observed (Fig. 6g–i).

**Fig. 10** Meridional momentum budget **a** pressure gradient, **b** Coriolis, **c** horizontal advection, and **d** mixing terms (shaded;  $\text{m s}^{-1} \text{h}^{-1}$ ) and meridional wind exceeding  $8 \text{ m s}^{-1}$  (contour;  $\text{m s}^{-1}$ ) at 975 hPa averaged 2005–2009 from the 27 km WRF simulation. Land is shaded grey



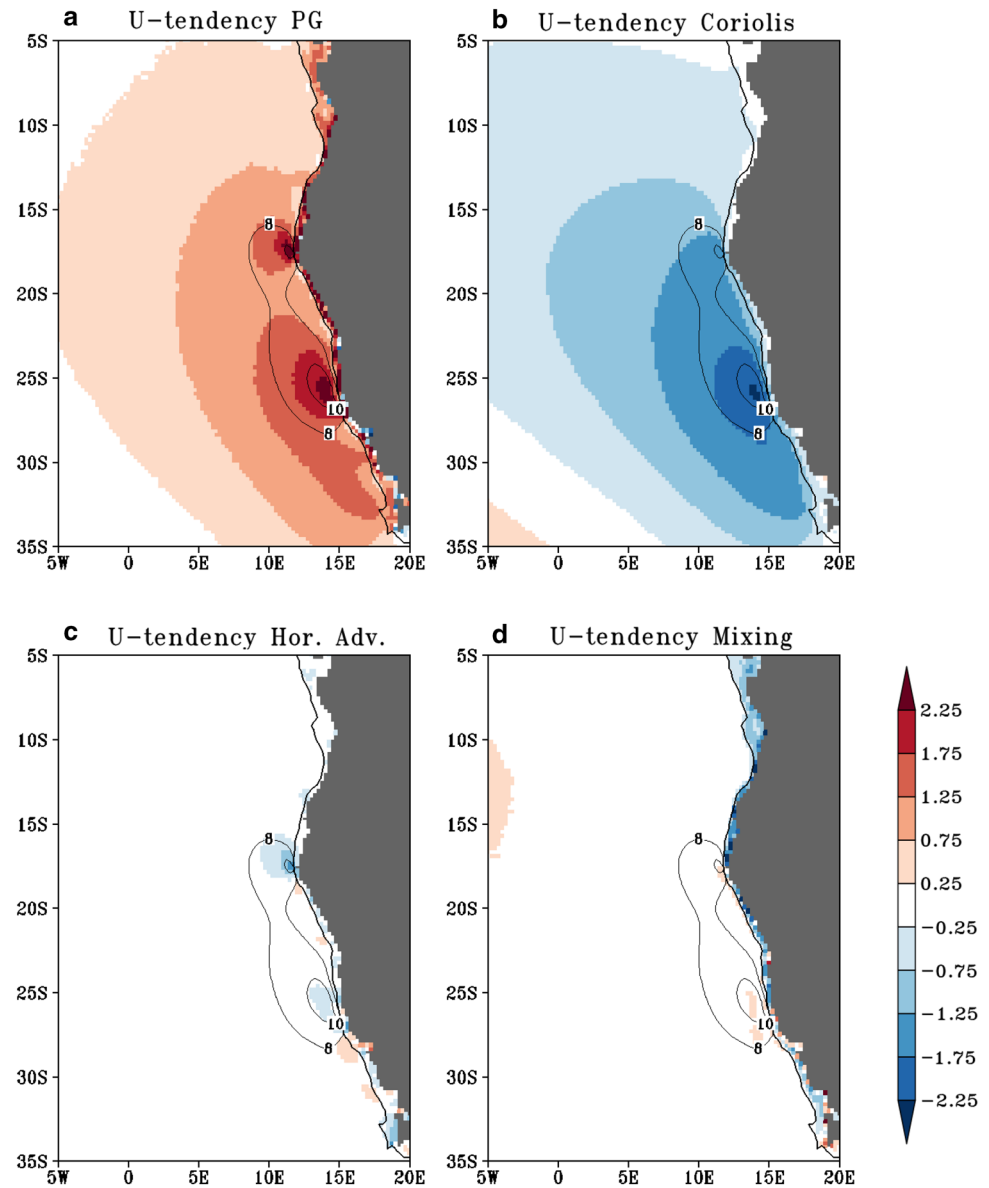
#### 4 Sensitivity of BLLCJ representation to model resolution

We next compare the simulated structure of the BLLCJ in regional climate model simulations of varying horizontal resolution and global models of the CMIP5 to the observational products presented in the previous section. The representation of the BLLCJ is highly dependent on model horizontal resolution. The double maximum structure seen in the SCOW (Fig. 7a) is generally reproduced in WRF simulations at 9, 27, and 81 km (Fig. 7b–d), whereas the WRF simulation at 243 km resolution (Fig. 7e) and the CMIP5 multi-model ensemble (Fig. 7f) fail to represent this structure and instead show a single broad maximum, similar to the coarse resolution reanalyses and CORE-II product (Fig. 3g–i). The latitude of the northern maximum is nearly the same between the SCOW and WRF 9, 21, and 81 km simulations, and tends to be stronger in the model

than observations. On the other hand, there is slightly more variability in the location of the southern maximum, with the 9 km WRF simulation (Fig. 7b) placing the maximum a few degrees of longitude offshore as in the SCOW (Fig. 7a), but the 27 and 81 km WRF simulations (Fig. 7c, d) placing the maximum closer to the coastline, as in several high resolution reanalyses (Fig. 3c–f). The lack or use of a convective parameterization results in a largely similar BLLCJ representation in 9 km resolution simulations (not shown). The vertical jet structure is also qualitatively similar between the higher resolution (9, 27, and 81 km) WRF simulations (not shown) and the higher resolution reanalyses (i.e., CFSR, JRA-55, MERRA, CFSR, ERA-Interim), and between the coarse resolution (243 km) WRF simulation (not shown) and the NCEP and NCEP-II reanalyses.

The near coast 10-m meridional wind profile through the northern BLLCJ maximum at  $17.5^{\circ}\text{S}$  near the ABF is also highly sensitive to model resolution. In all cases from 9 km

**Fig. 11** Zonal momentum budget **a** pressure gradient, **b** Coriolis, **c** horizontal advection, and **d** mixing terms (shaded;  $\text{m s}^{-1} \text{h}^{-1}$ ) and meridional wind exceeding  $8 \text{ m s}^{-1}$  (contour;  $\text{m s}^{-1}$ ) at 975 hPa averaged 2005–2009 from the 27 km WRF simulation. Land is shaded grey

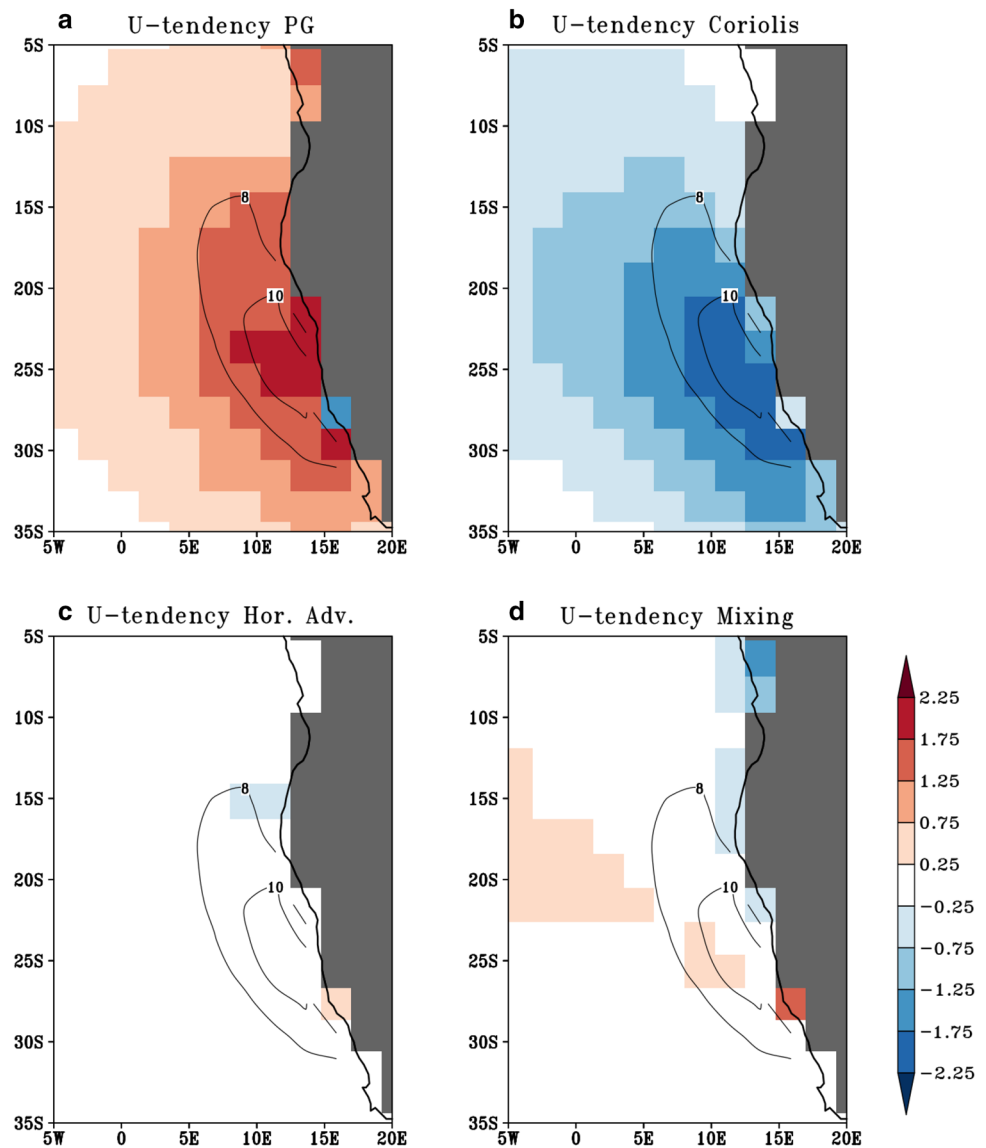


through 243 km resolution, the regional climate model places the maximum wind speed two grid points offshore from the coast (Fig. 8). We note that the 3 km simulation is not directly comparable with the others, as it was run for a short time period due to high computational cost. However, the 3 and 9 km resolution simulations do seem to converge on a solution in terms of the location of the maximum wind speed relative to the coast. Whether this wind profile matches that in nature remains an open question, due to sparse availability of in-situ wind observations in that region.

The differences among the near shore 10-m meridional wind from the WRF and CMIP5 simulations translate into considerable differences in the surface wind stress

curl that also depend highly on the model resolution (Fig. 9), as with the observational products. Among all of the simulations, the one at 9 km resolution (Fig. 9b) most closely reproduces the observed (Fig. 9a) spatial pattern of wind stress curl, including the local maximum at  $17.5^\circ\text{S}$  immediately adjacent to the coast. However, the high-resolution (9–81 km) model simulations (Fig. 9b–d), like the high-resolution reanalyses (Fig. 6b–f), overestimate the magnitude of the wind stress curl along the coast. The regional model at 243 km resolution (Fig. 9e) and the multi-model ensemble of CMIP5 global models (Fig. 9f), like the coarse resolution observational products (Fig. 6g–i), represent the wind stress curl poorly as a broad weak minimum.

**Fig. 12** Similar to Fig. 11, except from the 243 km WRF simulation



## 5 Dynamics of the Benguela LLCJ

### 5.1 Momentum balance

A momentum balance at the level of the jet maximum, 975 hPa, is presented to understand the factors that support the Benguela LLCJ. The momentum balance terms were calculated directly within the WRF dynamical solver, and residuals are relatively small (not shown). The meridional momentum budget is expressed as

$$\frac{\partial V}{\partial t} = -U \frac{\partial V}{\partial x} - V \frac{\partial V}{\partial y} - \frac{1}{\rho} \frac{\partial P}{\partial y} - fU + V_m \quad (1)$$

where, from left to right, terms represent local time rate of change, zonal advection, meridional advection, pressure gradient, Coriolis, and vertical and horizontal mixing ( $V_m$

).  $U$  is zonal wind vector,  $V$  is meridional wind vector,  $\rho$  is density of air,  $P$  is pressure, and  $f$  is Coriolis parameter.

The meridional momentum budget from the 27 km resolution WRF simulation averaged January 2005–December 2009 shows that the primary positive contribution in the Benguela jet region is from the pressure gradient term, with two maxima collocated with the BLLCJ maxima (Fig. 10a). The pressure gradient term is balanced by similar contributions from the Coriolis (Fig. 10b) and mixing (Fig. 10d) terms over the broad BLLCJ region and by localized contributions from the horizontal advection term over the jet maximum regions only, with negative and positive values south and north, respectively, of each jet maximum (Fig. 10c).

The zonal momentum budget is similarly expressed as

$$\frac{\partial U}{\partial t} = -U \frac{\partial U}{\partial x} - V \frac{\partial U}{\partial y} - \frac{1}{\rho} \frac{\partial P}{\partial x} + fV + U_m \quad (2)$$

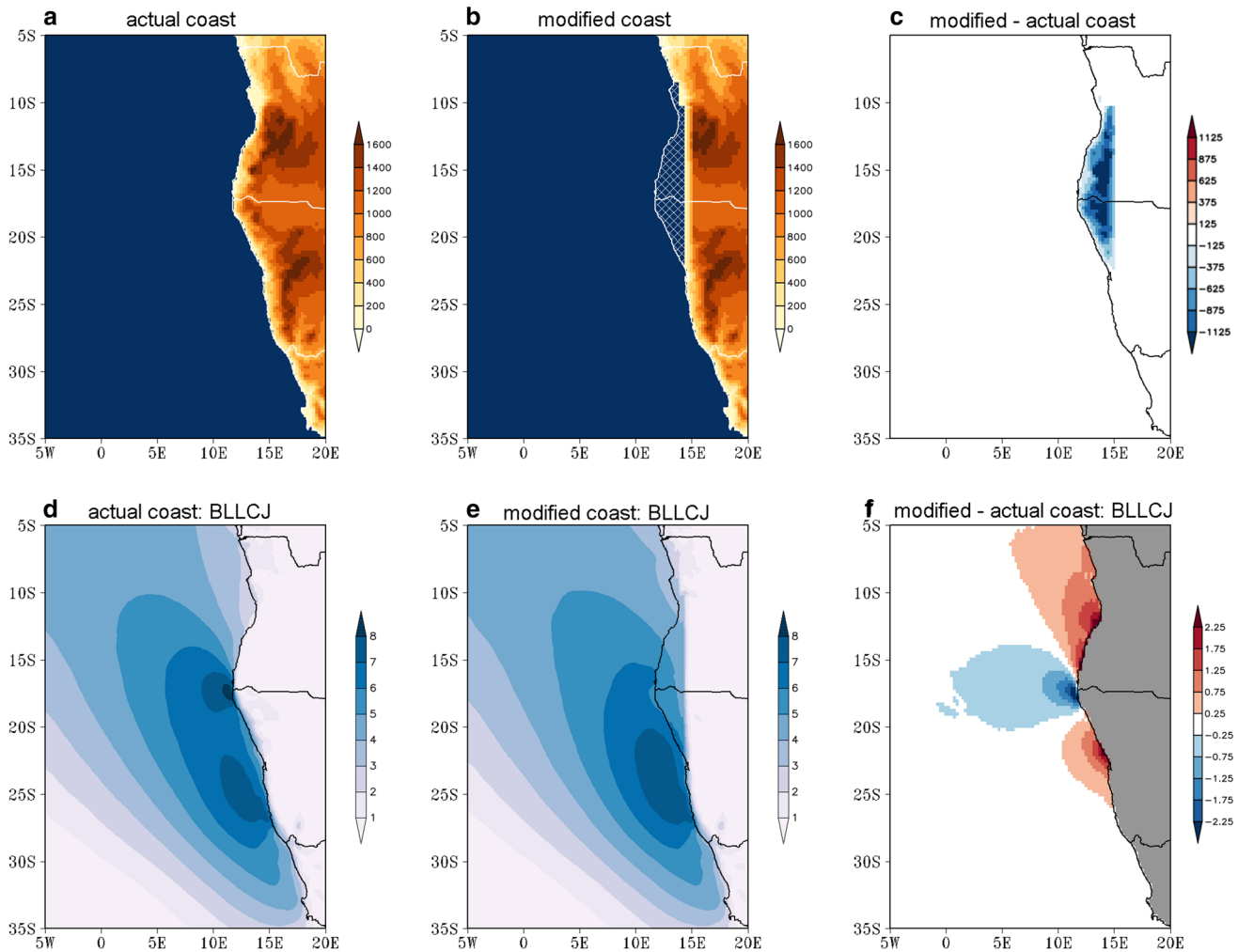


**Fig. 13** Terrain height (m; *shaded*) from 27 km WRF simulations with prescribed **a** actual and **b** modified coastline. *Blue* denotes ocean and *white hatching* denotes the region where land is changed to ocean. **c** The difference in terrain height (m) between the modi-

fied—actual coast simulations. Meridional wind at 10-m ( $\text{m s}^{-1}$ ) from the simulations with **d** actual coastline, **e** modified coastline and **f** the modified—actual coastline difference. *Grey shading* denotes land in (**f**)

Figure 11 shows the terms of the zonal momentum budget from the 27 km resolution WRF simulations. The pressure gradient term provides the main positive contribution to the zonal budget in the region of the Benguela LLCJ, and shows two maxima that coincide with the jet maxima (Fig. 11a). The balance in the jet region is primarily between the zonal pressure gradient and Coriolis terms (Fig. 11a, b), with a highly localized contribution from the non-linear horizontal advection term over the northern jet region (Fig. 11c), which is not resolved at 243 km resolution (Fig. 12c). In general the zonal mixing term is near-zero, except directly adjacent to the coast (Fig. 11d). The characteristics of the zonal momentum balance are qualitatively similar between the Benguela (Fig. 11) and South America LLCJs (Fig. 6 of Muñoz and Garreaud 2005), with the exception of the secondary horizontal advection

contribution in the northern maximum of the BLLCJ. As such, the zonal momentum budgets over both jet regions are approximately described by geostrophy, indicating that the meridional wind is approximately proportional to the zonal pressure gradient. By considering LLCJs as a geostrophically adjusted response to land-sea thermal contrast (Parish 2000), the location of LLCJs relative to the coast can be estimated by the Rossby radius of deformation, which is a function of MABL depth, Brunt-Väisälä frequency across the MABL inversion, and Coriolis parameter (Parish 2000; Ranjha et al. 2013). The June–August climatology of the BLLCJ from the ERA-Interim Reanalysis shows a northern BLLCJ maximum that extends 300 km offshore and is characterized by a Rossby radius of 240 km; owing to low terrain height from the coast to 100 km inland, the jet extends inland 100 km until it reaches steep terrain and



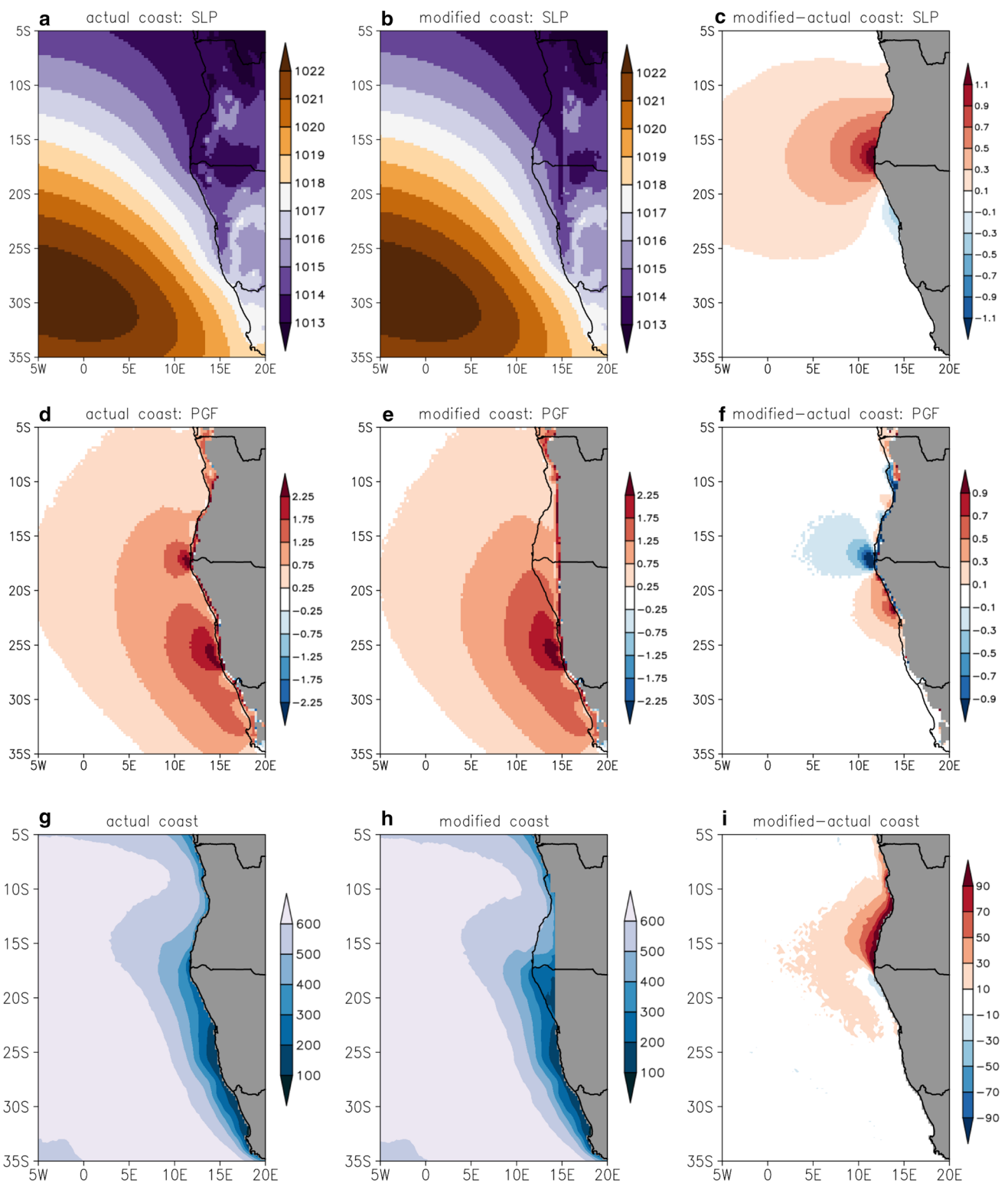


**Fig. 14** Sea-level pressure (hPa) from 27 km WRF simulations with (a) actual coastline, (b) modified coastline and (c) the modified—actual coastline difference. d, f Similar to (a–c), except for the zonal pressure gradient force momentum budget term ( $m\ s^{-1}\ h^{-1}$ ). g–i Simi-

lar to (a–c), except for marine boundary layer height (m). All panels are averaged January 2005 through December 2009. Grey shading indicates land in (c–i)

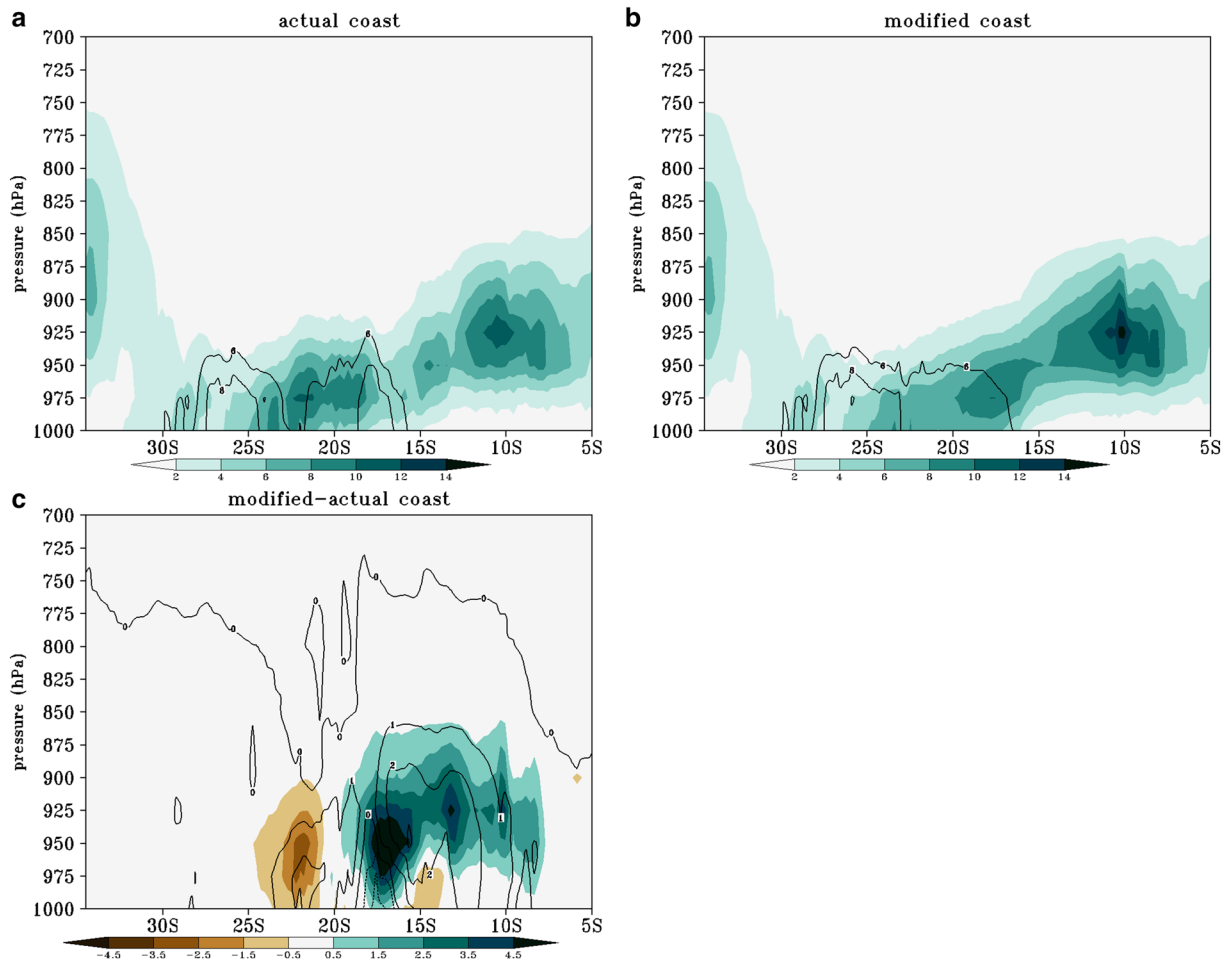


**Fig. 15** Vertical cross sections of cloud water mixing ratio ( $10^{-5}$  kg  $\text{kg}^{-1}$ ; shaded) and meridional wind ( $\text{m s}^{-1}$ ; contour) averaged over the first five ocean gridpoints away from the coastline (representing the approximately 1.2 longitude band adjacent to the coast) averaged

January 2005–December 2009 from 27 km resolution WRF simulations with prescribed **a** actual coastline, **b** modified coastline, and **c** the modified minus actual coastline difference. **a**, **b** Contour levels are 6, 8, and 10 m/s to emphasize the BLLCJ. **c** Contour levels are 1 m/s

is characterized by a wind maximum at the coast (Ranjha et al. 2013). In comparison, the December–February climatology shows a more offshore southern BLLCJ maximum. These differences in location of the BLLCJ maxima relative to the coast (Ranjha et al. 2013) are consistent with the BLLCJ structure seen in the SCOW satellite wind product and the 27 km resolution regional climate model simulation (Fig. 7a, c).

The representation of the zonal pressure gradient, like the Benguela LLCJ, is highly sensitive to model resolution. At 9 km (not shown), 27 km (Fig. 11a), and 81 km (not shown) resolutions, the WRF model produces two maxima in the zonal pressure gradient term, consistent with locations of the two BLLCJ maxima. It is clear that the misrepresentation of the BLLCJ as a single broad maximum in the coarse 243 km resolution simulation is related to the poor representation of the zonal pressure gradient

term (Fig. 12a). It seems that between the 100 and 200 km range, resolution becomes too coarse to resolve the gradients needed to support the detailed structure of the Benguela LLCJ.

## 5.2 Benguela LLCJ structure and coastal geometry

One robust feature of the BLLCJ in all high-resolution observational products, reanalyses, and model simulations is the anchoring of the northern jet maximum at approximately  $17.5^{\circ}\text{S}$  (Figs. 3a–f, 7b–d). In this section we investigate what determines the existence of the double maximum structure of the Benguela LLCJ and the location of the northern maximum. We test the hypothesis that the northern BLLCJ maximum is supported by the convex geometry of the coastline near  $17.5^{\circ}\text{S}$  by comparing WRF simulations at 27 km resolution with prescribed actual

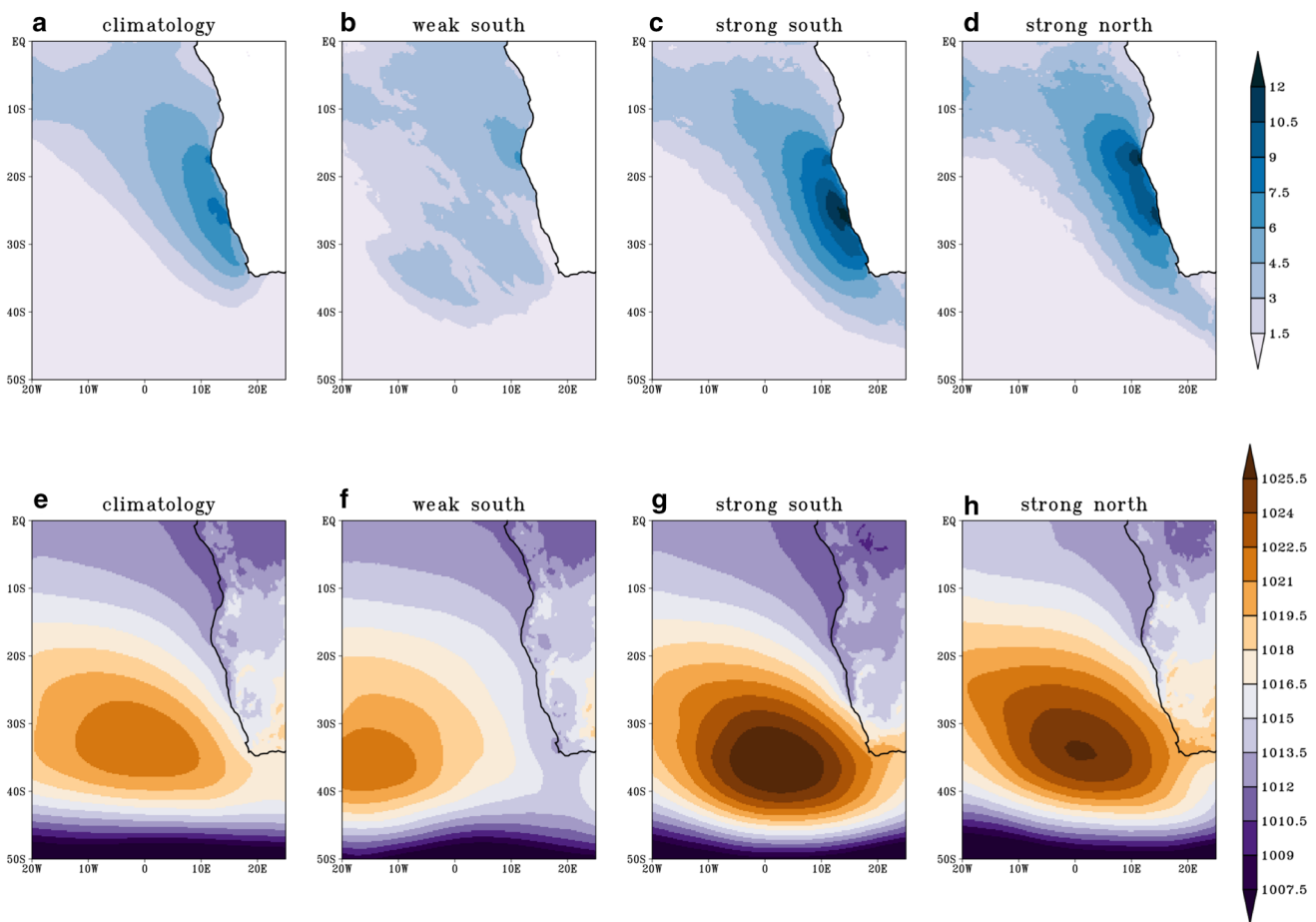


**Fig. 16** Meridional wind at 10-m ( $\text{m s}^{-1}$ ) from the WRF simulation at 27 km horizontal resolution from the March 2005–2014 **a** climatology and March composites of **b** weak southern maximum events,

**c** strong southern maximum events, and **d** strong northern maximum events. **e–h** Similar to (**a–d**), except for sea-level pressure (hPa). *White shading indicates land in (a–d)*

and modified coastal boundaries (Fig. 13a–c). The “modified coast” experiment alters the coastline near  $17.5^{\circ}\text{S}$  (Fig. 13b) such that terrain height is set to zero over the region where land is changed to ocean, and SST over the new ocean area is extrapolated from surrounding ocean points. We note that the coastal topography in the modified coast experiment remains steep, one of the known conditions to support LLCJs. The northern jet maximum that is present in the “actual coastline” simulation (Fig. 13d) is absent in response to altering the convex region at  $17.5^{\circ}\text{S}$  (Fig. 13e). The wind speed reduction near  $17.5^{\circ}\text{S}$  due to modifying the coast (Fig. 13f) is indicative of the absence of the hydraulic expansion fan characteristic of the case with the convex coastline. Furthermore, when the coastal geometry is altered, wind speed is enhanced upwind of the region where the convex coastline was removed, near  $25^{\circ}\text{S}$ – $20^{\circ}\text{S}$ , indicating the absence of the hydraulic jump characteristic of the case with the convex coastline. These responses in 10-m wind over the ocean back the hypothesis that the northern BLLCJ maximum is supported by

the convex coastal geometry through hydraulic theory arguments.

As demonstrated in the previous section, there is a strong relationship between the low-level zonal pressure gradient and the BLLCJ, therefore the sea-level pressure response to the altered coastline is presented. The large-scale South Atlantic subtropical high simulated in the actual coastline case (Fig. 14a) is unchanged due to altering the coast (Fig. 14b, c). However, there is a strong local response in sea-level pressure over and north of the northern jet maximum region such that altering the coast relaxes the low pressure over the ABF region seen in the actual coastline case (Fig. 14a–c). Along with the local response in sea-level pressure is a reduction in the 975 hPa zonal pressure gradient over the northern jet maximum region and an enhancement in the gradient south of the northern jet maximum region (Fig. 14f). In fact, the 975 hPa zonal pressure gradient maximum over the ABF in the actual coastline simulation (Fig. 14d) is entirely eliminated due to altering the coastline (Fig. 14e). These changes in low-level zonal

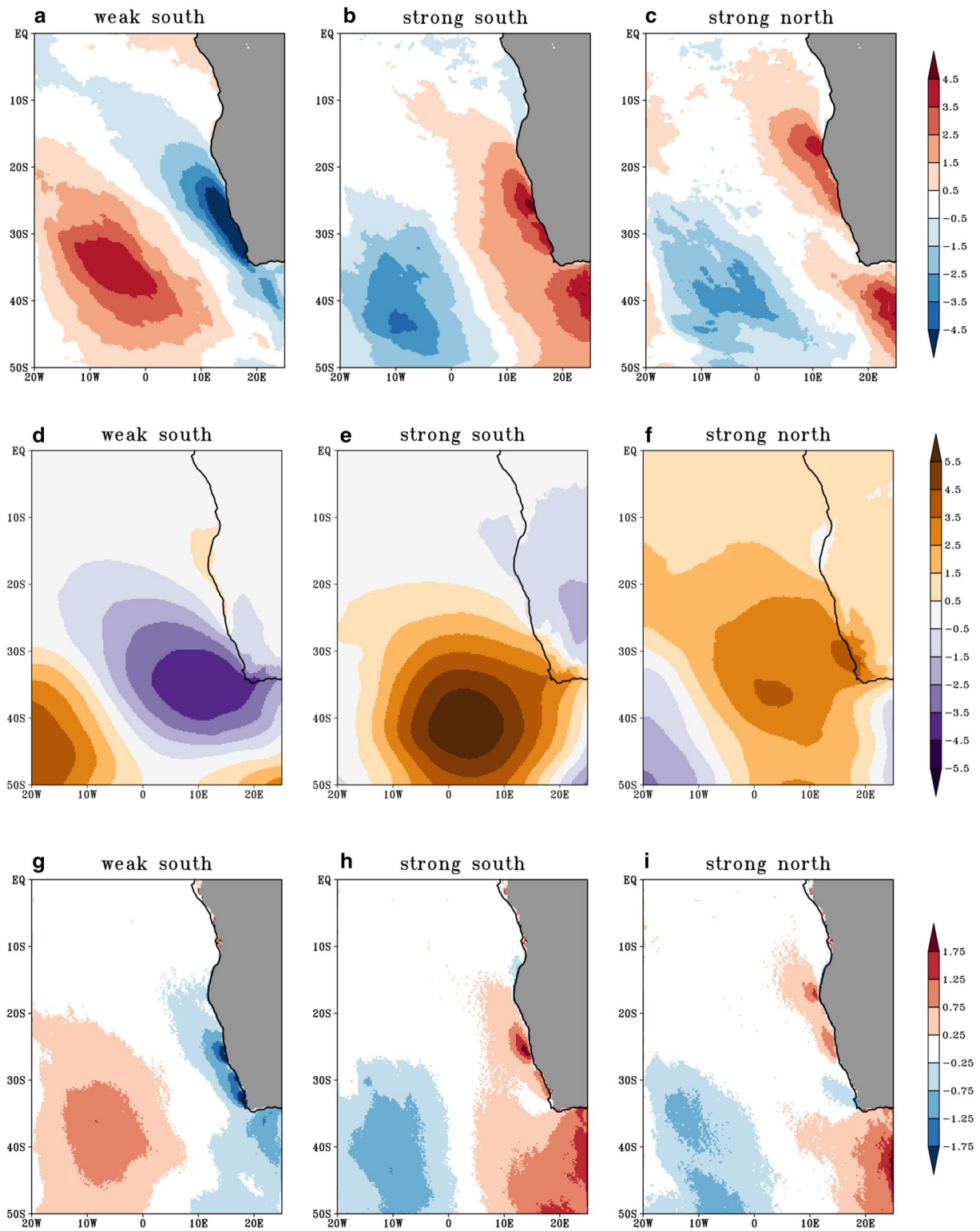


**Fig. 17** The anomaly in meridional wind at 10-m ( $\text{m s}^{-1}$ ), expressed as the difference from the climatology, from a WRF simulation at 27 km resolution from the March 2005–2014 composite of **a** weak southern maximum events, **b** strong southern maximum events, and

**c** strong northern maximum events. **(d, f)** Similar to **(a–c)**, except for sea-level pressure (hPa). **(g–i)** Similar to **(a–c)**, except for the zonal momentum budget pressure gradient term ( $\text{m s}^{-1} \text{h}^{-1}$ ). Grey shading indicates land in **(a–c)** and **(g–i)**

pressure gradient correspond to the response in the BLLCJ in both spatial pattern and magnitude (Figs. 13d–f, 14d–f). The dynamical changes in the altered coastline experiment further support the idea that the northern BLLCJ maximum is supported by the convex coastal geometry near the ABF. By removing the convex portion of the coastline, the northern wind and zonal pressure gradient maxima associated with a hydraulic expansion fan are eliminated.

A thinning of the marine atmospheric boundary layer is characteristic of hydraulic expansion fans, and is linked to a reduction in low-level cloud cover through adiabatic warming associated with descending motion. Together with the absence of the northern BLLCJ maximum in response to altering the coastal geometry, MABL height is increased in the vicinity of and north of the northern maximum (Fig. 14g–i), adding support to the idea that the northern BLLCJ maximum is supported by the convex coastal geometry. The response in low-level clouds is also consistent with this hypothesis. Vertical cross sections along an approximately 1.2° longitude band off the African coastline show a relative minimum in low-level clouds concurrent with the Benguela LLCJ northern maximum in the “actual coastline” simulation (Fig. 15a). This is expected with the thinning of the MABL and cloud cover reduction associated with an expansion fan occurring upstream of convex coastal geometry. In the “altered coast” case, the northern jet maximum is absent and there is no corresponding minimum in low-level cloud cover (Fig. 15b). This pronounced effect is apparent in the difference fields (Fig. 15c), and offers further evidence that the convex coastal geometry supports the existence of the northern jet maximum at 17.5°S.

## 6 Large-scale controls on Benguela LLCJ variability

The Benguela LLCJ is marked by substantial intraseasonal variability, with a peak in QuikSCAT-derived surface wind stress over 10°S–23.5°S at the 6–16 day period (Risien et al. 2004). In order to understand how large-scale atmospheric conditions support Benguela LLCJ events, we define BLLCJ indices based on the 10-m meridional wind for the northern and southern jet maxima. The northern jet index is area-averaged over 19°S–16.1°S and 8°E–11.7°E, and the southern jet index over 27.9°S–22°S and 10°E–15.5°E. The time series of jet indices are computed using the daily area-averaged 10-m meridional wind from the 27 km resolution regional climate model simulation over the 2005–2014 period. The Benguela jet is classified as “weak” or “strong” when the daily jet index value is below, or exceeds, one standard deviation of the mean index value over the entire 2005–2014 period. All days in which the jet is “weak” or

“strong” are collected and averaged to form composites of exceptionally strong jet events or non-events.

Composites of the BLLCJ are considered during March, when the coastal SST bias in coupled models tends to develop rapidly (Richter and Xie 2008; Patricola et al. 2012). The composites are formed for one month, rather than on the annual timescale, so that the influence of the seasonal cycle is removed. During the March climatology, which includes all days without regard to jet event classification, the Benguela LLCJ is characterized by maxima over both the northern and southern regions (Fig. 16a) and the South Atlantic subtropical high is centered near 35°S and 0° longitude (Fig. 16e). During times characterized by weak jet events over the southern region (Figs. 16b, 17a; representing 12% of the days in March 2005–2014), the center of the subtropical high is shifted westward (Fig. 16f), placing negative sea-level pressure anomalies off the coast of western South Africa (Fig. 17d) with a corresponding reduction in the zonal pressure gradient at 975 hPa (Fig. 17g) that coincides with the 10-m meridional wind anomalies (Fig. 17a). Likewise, in the composite of strong jet events over the southern region (Figs. 16c, 17b; representing 10% of the days in March), the subtropical high is shifted eastward and intensified (Fig. 16g), with positive sea-level pressure anomalies over the near-coastal ocean confined primarily south of 27°S (Fig. 17e) leading to anomalies in the zonal pressure gradient momentum budget term that are greatest over the southern region (Fig. 17h).

During the times in March when the northern BLLCJ maximum is strong (Figs. 16d, 17c), the subtropical high is also strengthened and shifted northeastward (Fig. 16h) with subtle differences in the sea-level pressure anomalies (Fig. 17f) that support a maximum strengthening of the zonal pressure gradient over the northern jet region (Fig. 17i). During times when the northern or southern jet maximum is strong, there tends to be concurrent strengthening of wind speed in the other jet maximum region (Fig. 17b, c). In general, a strengthening and eastward shift of the South Atlantic subtropical high, sometimes with concurrent negative sea level pressure anomalies over South Africa, are associated with strong BLLCJ events throughout the year. This link between the large and smaller scale is also apparent in the observed connection between variations in low-level winds off the Oregon coast and variability in the North Pacific High (Bane et al. 2005).

## 7 Conclusions

The detailed structure of surface wind stress and wind stress curl associated with the Benguela low-level coastal jet plays a critical role in driving the Benguela coastal upwelling system and shaping the regional SST pattern

(Colberg and Reason 2006; Small et al. 2015). Errors in representation of the Benguela LLCJ are a major source of the persistent warm coastal SST bias (Grodsky et al. 2012; Small et al. 2015; Kurian et al. 2016, in preparation) seen in generations of global coupled atmosphere–ocean climate models (Richter and Xie 2008; Xu et al. 2014b). Here we examined the structure of the Benguela LLCJ in a suite of observational products, reanalyses, and climate models. The Benguela LLCJ representation among these datasets falls into two classifications. In finer resolution products and models, including the “closest to the truth” satellite-based SCOW and CCMP, several atmospheric reanalyses, and regional climate model simulations at 9, 27, and 81 km resolution, the BLLCJ is characterized by two near-shore maxima, one near the ABF at 17.5°S, and the other near 25–27.5°S. On the other hand, coarse resolution reanalyses and models (greater than about 2°), including the CORE-II dataset, a multi-model ensemble from the CMIP5 global models, and a regional climate model at 243 km resolution, represent the Benguela LLCJ poorly, with a single, broad, more offshore jet maximum. These errors in jet representation in coarse resolution products translate into substantial biases in coastal SST representation, on the order of 4 °C; however, coastal SST biases were greatly improved by forcing a regional ocean model with atmospheric data from the 9 and 27 km WRF simulations presented in this paper (Kurian et al. 2016, in preparation). The ability of regional climate models to realistically represent scales finer than those of typical reanalyses and to skillfully reproduce observed interannual variability (e.g., Patricola et al. 2014) suggests there is a good potential for regional climate models to generate ocean model forcings that can advance our understanding of regional coupled air-sea processes. Still, we emphasize that in-situ observations of surface wind in the southeastern tropical Atlantic are needed, as land contamination in satellite observations generates uncertainty in near-coast surface wind and wind stress curl.

The dynamics of the Benguela LLCJ were investigated with the ultimate motivation of reducing southeastern tropical Atlantic SST biases, which can hinder our ability to represent, for example, the West African monsoon (Hsu et al. 2016). We found similarities between the relatively understudied Benguela LLCJ and the well-observed South American and California LLCJs. Both LLCJs occur over eastern boundary coastal upwelling regions and are supported by a near-surface pressure gradient that forms perpendicular to the coast, where a cool stable marine boundary layer exists over cold upwelling SST and is adjacent to warm land with steep coastal terrain. Momentum budget analysis of the Benguela LLCJ revealed approximate geostrophy in the zonal direction, with the climatological mean meridional wind nearly proportional to the zonal pressure gradient, similar to the South American LLCJ. The

regional climate model at the coarse resolution of 243 km was unable to resolve the two maxima in the Benguela jet and low-level zonal pressure gradient.

One marked difference between the South American and Benguela LLCJs is the structure, with the jets characterized by a single maximum and double maxima, respectively. The smaller-scale structure of the LLCs is supported by the coastal geometry, which is smooth in the South American case and more detailed in the African case. Regional climate model experiments with a modified coastline indicate that the northern maximum of the Benguela LLCJ, and associated local minimum in low-level cloud cover, occurs in association with a hydraulic expansion fan that arises downwind of the convex coastal geometry. This suggests that realistic model representation of the Benguela LLCJ relies on a properly resolved coastline.

The Benguela LLCJ displays significant variability on the intraseasonal timescale that is driven by variability in the South Atlantic subtropical high. Strong jet events tend to occur when the subtropical high is relatively intense and shifted towards the African continent. Whether the jet strengthens most in the northern or southern region depends on more subtle shifts in the subtropical high.

The understanding gained by this investigation of the Benguela low-level coastal jet is anticipated to contribute significantly towards reducing the severe warm coastal SST biases that have persisted in generations of coupled models, and advancing our seasonal and future climate projection capability. Additional research to investigate connections between Benguela LLCJ events and coastal SST and the ABF location would provide useful information on interactions between atmosphere and ocean in this coastal upwelling region. The connections between the Benguela LLCJ and the large-scale circulation suggest that projected future changes in land-sea contrast and the south Atlantic subtropical high may provide some insight towards expected changes in upwelling in the Benguela system due to climate change, even in climate models that do not resolve the Benguela LLCJ well.

**Acknowledgements** This research was supported by U.S. National Science Foundation Grant OCE-1334707 and used the Extreme Science and Engineering Discovery Environment (XSEDE), which is supported by National Science Foundation Grant ACI-1053575. High-performance computing resources provided by the Texas Advanced Computing Center (TACC) at The University of Texas at Austin and by the Texas A&M Supercomputing Facility. SCOW, NCEP CFSR, JRA-55, ECMWF-Interim, NCEP Reanalysis, and NCEP-II Reanalysis available at the Research Data Archive at the National Center for Atmospheric Research, Computational and Information Systems Laboratory, Boulder, CO. CCMP and GHRSSST MUR SST available at <ftp://podaac.jpl.nasa.gov>. MERRA available from NASA's Global Modeling and Assimilation Office (GMAO) and the Goddard Earth Sciences Data and Information Services Center (GES DISC). CORE-II available at <http://data1.gfdl.noaa.gov/nomads/forms/core/COREv2.html>. NOAA\_OI\_SST\_V2 data provided by the NOAA/

OAR/ESRL PSD, Boulder, Colorado, USA, at <http://www.esrl.noaa.gov/psd>. Figures created using the Grid Analysis and Display System (GrADS), GrADS functions by Chihiro Kodama, and <http://colorbrewer2.org/>. The authors thank J. Kurian, R. Saravanan, R. J. Small, and P. Zuidema for helpful discussions and three anonymous reviewers for their comments that have helped improve the paper.

## References

- Atlas R, Hoffman RN, Ardizzone J, Leidner SM, Jusem JC, Smith DK, Gombos D (2011) A cross-calibrated, multiplatform ocean surface wind velocity product for meteorological and oceanographic applications. *Bull Amer Meteor Soc* 92:157–174
- Bane JM, Levine MD, Samelson RM, Haines SM, Meaux MF, Perlin N, Kosro PM, Boyd T (2005) Atmospheric forcing of the Oregon coastal ocean during the 2001 upwelling season. *J Geophys Res* 110:C10S02
- Bearsley RC, Dorman CE, Friehe CA, Rosenfeld LK, Winant CD (1987) Local atmospheric forcing during the coastal ocean dynamics experiment: 1. A description of the marine boundary layer and atmospheric conditions over a northern California upwelling region. *J Geophys Res* 92(C2):1467–1488
- Chang C-Y, Carton JA, Grodsky SA, Nigam S (2007) Seasonal climate of the tropical Atlantic sector in the near community climate system model 3: error structure and probable causes of errors. *J Climate* 20:1053–1070
- Chin TM, Vazquez J, Armstrong E (2013) A multi-scale, high-resolution analysis of global sea surface temperature. In *Algorithm Theoretical Basis Document, Version 1.3*, Pasadena, CA: Jet Propulsion Laboratory p 13
- Colberg F, Reason CJC (2006) A model study of the Angola Benguela frontal zone: sensitivity to atmospheric forcing. *Geophys Res Lett* 33:L19608
- Dee DP et al. (2011) The ERA-Interim reanalysis: configuration and performance of the data assimilation system. *QJR Meteorol Soc* 137:553–597
- DeWitt DG (2005) Diagnosis of the tropical Atlantic near-equatorial SST bias in a directly coupled atmosphere–ocean general circulation model. *Geophys Res Lett* doi:10.1029/2004GL021707
- Dorman CE (1985) Hydraulic control of the northern California marine layer. *Eos Trans Amer Geophys Union* 66:914
- Dorman CE, Koračin D (2008) Response of the summer marine layer flow to an extreme California coastal bend. *Mon Weather Rev* 136(8):2894–2992
- Fennel W, Junker T, Schmidt M, Mohrholz V (2012) Response of the Benguela upwelling systems to spatial variations in the wind stress. *Cont Shelf Res* 45:65–77
- Garreaud RD, Muñoz RC (2005) The low-level jet off the west coast of subtropical South America: structure and variability. *Mon Weather Rev* 133:2246–2261
- Gerber H, Chang S, Holt T (1989) Evolution of a marine boundary-layer jet. *J Atm Sci* 46(10):1312–1326
- Grodsky SA, Carton JA, Nigam S, Okumura YM (2012) Tropical Atlantic biases in CCSM4. *J Climate* 25(11):3684–3701
- Hazeleger W, Harsma RJ (2005) Sensitivity of tropical Atlantic climate to mixing in a coupled ocean–atmosphere model. *Clim Dyn* 25:387–399
- Hsu W-C, Chang P, Patricola CM (2016) Quantifying the impact of sea surface temperature biases on simulated tropical cyclones (in preparation)
- Huang B, Hu Z-Z, Jha B (2007) Evolution of model systematic errors in the Tropical Atlantic Basin from coupled climate hindcasts. *Clim Dyn* 28:661–682
- Junker T, Schmidt M, Mohrholz V (2015) The relation of wind stress curl and meridional transport in the Benguela upwelling system. *J Mar Syst* 143:1–6
- Kalnay E et al (1996) The NCEP/NCAR 40-year reanalysis project. *Bull Amer Meteor Soc* 77:437–471
- Kanamitsu M, Ebisuzaki W, Woollen J, Yang S-K, Hnilo JJ, Fiorino M, Potter GL (2002) NCEP–DOE AMIP-II reanalysis (R-2). *Bull Amer Meteor Soc* 83:1631–1643
- Kobayashi S et al (2015) The JRA-55 reanalysis: general specifications and basic characteristics. *J Met Soc of Japan* 93:5–48
- Kurian J, Patricola CM, Chang P, Montuoro R, Li P (2016) Impact of the Benguela low-level coastal jet on Southeast tropical Atlantic SST Bias (in preparation)
- Large WG, Danabasoglu G (2006) Attribution and Impacts of Upper-Ocean Biases in CCSM3. *J Climate* 19:2325–2346
- Large WG, Yeager SG (2008) The global climatology of an interannually varying air–sea flux data set. *Clim Dyn* 33:341–364.
- Lutjeharms JRE, Meeuwis JM (1987) The extent and variability of South-East Atlantic upwelling. *S Afr J Mar Sci* 5:51–62
- Milinski S, Bader J, Haak H, Siongco AC, Jungclaus JH (2016) High atmospheric horizontal resolution eliminates the wind-driven coastal warm bias in the southeastern tropical Atlantic. *Geophys Res Lett* 43(19):10455–10462
- Muñoz RC, Garreaud RD (2005) Dynamics of the low-level jet off the west coast of subtropical South America. *Mon Weather Rev* 133:3661–3677
- Neiburger M, Johnson DS, Chien CW (1961) Studies of the structure of the atmosphere over the eastern Pacific Ocean in the summer. The inversion over the eastern north Pacific ocean, University of California Press, California, pp 1–94
- Nicholson SE (2010) A low-level jet along the Benguela Coast, an integral part of the Benguela current ecosystem. *Clim Change* 99:613–624
- Parish TR (2000) Forcing of the summertime low-level jet along the California coast. *J Appl Meteorol* 39:2421–2433
- Patricola CM, Li M, Xu Z, Chang P, Saravanan R, Hsieh J-S (2012) An investigation of tropical Atlantic bias in a high-resolution coupled regional climate model. *Clim Dyn* 39(9–10):2443–2463
- Patricola CM, Saravanan R, Chang P (2014) The impact of the El Niño–southern oscillation and Atlantic meridional mode on seasonal Atlantic tropical cyclone activity. *J Clim* 27:5311–5328
- Rahn DA, Parish TR (2007) Diagnosis of the forcing and structure of the coastal jet near Cape Mendocino using in situ observations and numerical simulations. *J Appl Meteorol Climatol* 46(9):1455–1468
- Ranjha R, Svensson G, Tjernström M, Semedo A (2013) Global distribution and seasonal variability of coastal low-level jets derived from ERA-Interim reanalysis. *Tellus A* 65:20412
- Reynolds RW, Rayner NA, Smith TM, Stokes DC, Wang W (2002) An improved in situ and satellite SST analysis for climate. *J Climate* 15:1609–1625
- Richter I (2015) Climate model biases in the eastern tropical oceans: causes, impacts and ways forward. *WIREs Clim Change* 6:345–358.
- Richter I, Xie S-P (2008) On the origin of equatorial Atlantic biases in coupled general circulation models. *Clim Dyn* 31:587–598
- Richter I, Xie S-P, Wittenberg AT, Masumoto Y (2012) Tropical Atlantic biases and their relation to surface wind stress and terrestrial precipitation. *Clim Dyn* 35(5):985–1001
- Rienecker MM et al (2011) MERRA: NASA’s modern-era retrospective analysis for research and applications. *J Climate* 24:3624–3648
- Risien CM, Chelton DB (2008) A global climatology of surface wind and wind stress fields from eight years of Quikscat scatterometer data. *J Phys Oceanogr* 38:2379–2413

- Risien CM, Reason CJC, Shillington FA, Chelton DB (2004) Variability in satellite winds over the Benguela upwelling system during 1999–2000. *J Geophys Res* 109:C03010
- Rogers DP et al (1998) Highlights of coastal waves 1996. *Bull Am Meteorol Soc* 79:1307–1326
- Rouault M, Illig S, Bartholomae C, Reason CJC, Bentamy A (2007) Propagation and origin of warm anomalies in the Angola Benguela upwelling system in 2001. *J Marine Syst* 68(3–4):473–488
- Saha S et al (2010) The NCEP climate forecast system reanalysis. *Bull Amer Meteor Soc* 91:1015–1057
- Samelson RM (1992) Supercritical marine-layer flow along a smoothly Varying Coastline. *J Atmos Sci* 49:1571–1584
- Skamarock WC et al (2008) A time-split nonhydrostatic atmospheric model for weather research and forecasting applications. *J Comput Phys* 227(7):3465–3485
- Small RJ, Curchitser E, Hedstrom K, Kauffman B, Large WG (2015) The Benguela upwelling system: quantifying the sensitivity to resolution and coastal wind representation in a global climate model. *J Clim*. doi:[10.1175/JCLI-D-15-0192.1](https://doi.org/10.1175/JCLI-D-15-0192.1)
- Taylor KE, Stouffer RJ, Meehl GA (2012) An overview of CMIP5 and the experiment design. *Bull Am Meteorol Soc* 93:485–498
- Toniazzo T, Woolnough S (2014) Development of warm SST errors in the southern tropical Atlantic in CMIP5 decadal hindcasts. *Clim Dyn* 43:2889–2913.
- Wahl S, Latif M, Park W, Keenlyside N (2011) On the tropical atlantic SST warm bias in the kiel climate model. *Clim Dyn* 36:891–906
- Winant CD, Dorman CE, Friehe CA, Beardsley RC (1988) The marine layer off Northern California: an example of supercritical channel flow. *J Atmos Sci* 45:3588–3605
- Xu Z, Li M, Patricola CM, Chang P (2014a) Oceanic origin of south-east tropical Atlantic biases. *Clim Dyn* 43(11):2915–2930
- Xu Z, Chang P, Richter I, Kim W, Tang G (2014b) Diagnosing south-east tropical Atlantic SST and ocean circulation biases in the CMIP5 ensemble. *Clim Dyn* 43:3123–3145.
- Yang JX, McKague DS, Ruf CS (2014) Land contamination correction for passive microwave radiometer data: demonstration of wind retrieval in the great lakes using SSM/I. *J Atmos Oceanic Technol* 31(10):2094–2113
- Zemba J, Friehe CA (1987) The marine atmospheric boundary layer jet in the coastal ocean dynamics experiment. *J Geophys Res* 92(C2):1489–1496
- Zuidema P et al (2016) Challenges and prospects for reducing coupled climate model SST biases in the eastern tropical Atlantic and Pacific oceans: the U.S. CLIVAR Eastern Tropical Oceans Synthesis working group. *BAMS*. doi:[10.1175/BAMS-D-15-00274.1](https://doi.org/10.1175/BAMS-D-15-00274.1)